

THE EFFECT OF FIBER COLLISIONS ON THE GALAXY POWER SPECTRUM MULTIPOLES

CHANGHOON HAHN¹, ROMAN SCOCCIMARRO¹, MICHAEL R. BLANTON¹, JEREMY L. TINKER¹ SERGIO RODRÍGUEZ-TORRES^{2,3,4}

Draft version September 8, 2016

ABSTRACT

Fiber-fed multi-object spectroscopic surveys, with their ability to collect an unprecedented number of redshifts, currently dominate large-scale structure studies. However, physical constraints limit these surveys from successfully collecting redshifts from galaxies too close to each other on the focal plane. This ultimately leads to significant systematic effects on galaxy clustering measurements. Using simulated mock catalogs, we demonstrate that fiber collisions have a significant impact on the power spectrum, $P(k)$, monopole and quadrupole that exceeds sample variance at scales smaller than $k \sim 0.1 h/\text{Mpc}$.

We present two methods to account for fiber collisions in the power spectrum. The first, statistically reconstructs the clustering of fiber collided galaxy pairs by modeling the distribution of the line-of-sight displacements between them. It also properly accounts for fiber collisions in the shot-noise correction term of the $P(k)$ estimator. Using this method, we recover the true $P(k)$ monopole of the mock catalogs with residuals of $< 0.5\%$ at $k = 0.3 h/\text{Mpc}$ and $< 4\%$ at $k = 0.83 h/\text{Mpc}$ – a significant improvement over existing correction methods. The quadrupole, however, does not improve significantly.

The second method models the effect of fiber collisions on the power spectrum as a convolution with a configuration space top-hat function that depends on the physical scale of fiber collisions. It directly computes theoretical predictions of the fiber-collided $P(k)$ multipoles and reduces the influence of smaller scales to a set of nuisance parameters. Using this method, we reliably model the effect of fiber collisions on the monopole and quadrupole down to the scale limits of theoretical predictions. The methods we present in this paper will allow us to robustly analyze galaxy power spectrum multipole measurements to much smaller scales than previously possible.

Subject headings: cosmology: observations – cosmology: large-scale structure of universe – galaxies: halos – galaxies: statistics

1. INTRODUCTION

Cosmological measurements such as galaxy clustering statistics are no longer dominated by uncertainties from statistical precision, but from systematic effects of the measurements. This is a result of the millions of redshifts to distant galaxies that have been obtained through redshift surveys such as the 2dF Galaxy Redshift Survey (2dFGRS; Colless 1999) and the Sloan Digital Sky Survey III Baryon Oscillation Spectroscopic Survey (SDSS-III BOSS; Anderson et al. 2012; Dawson et al. 2013). Current surveys, such as the Extended Baryon Oscillation Spectroscopic Survey (eBOSS; Dawson et al. 2015), and future surveys such as the Dark Energy Survey Instrument (DESI; Schlegel et al. 2011; Morales et al. 2012; Makarewicz et al. 2014), and the Subaru Prime Focus Spectrograph (PFS; Takada et al. 2014), will continue to collect many more million redshifts, extending our measurements to unprecedented statistical precision. These completed and future surveys, all use and will use fiber-fed spectrographs.

For each galaxy, a fiber is used to obtain a spectroscopic redshift. However, the physical size of the fiber housing and other physical constraints limit how well any of these surveys can observe close pairs of galaxies. In the SDSS, if two galaxies are located within the fiber collision angular scale from one another on the sky, separate fibers cannot be placed adjacently to observe them simultaneously (Yoon et al. 2008). In these situations, only a single redshift is measured. With redshifts of galaxies in close angular proximity missing from the sample, any clustering statistic probing these scales will be systematically affected.

As our cosmological surveys extend further to higher redshifts, the systematic effect becomes more severe. The fiber collision angular scale corresponds to a larger comoving scale at higher redshift, thereby affecting our measurements on larger scales. BOSS, in particular, has an angular fiber collision scale of $62''$. This corresponds to $\sim 0.43 \text{ Mpc}/h$ at the center of the survey's redshift range; fiber-collided galaxies account for $\sim 5\%$ of the galaxy sample (Anderson et al. 2012; Reid et al. 2012; Guo et al. 2012). While this may seem like a relatively small fraction of redshifts, its effect on clustering measurements such as the power spectrum and bispectrum is significant and needs to be accounted for in order to probe mildly non-linear scales. Unfortunately, future spectroscopic surveys such as DESI, which will use robotic fiber positioner technology, will be subject

¹ Center for Cosmology and Particle Physics, Department of Physics, New York University, 4 Washington Place, New York, NY 10003; chh327@nyu.edu

² Instituto de Física Teórica, (UAM/CSIC), Universidad Autónoma de Madrid, Cantoblanco, E-28049 Madrid, Spain

³ Campus of International Excellence UAM+CSIC, Cantoblanco, E-28049 Madrid, Spain

⁴ Departamento de Física Teórica M8, Universidad Autónoma de Madrid, Cantoblanco, E-28049, Madrid, Spain

to similar effects. Therefore, accounting for the effects of fiber collisions will remain a crucial and unavoidable challenge for analyzing clustering measurements.

To correct for fiber collisions, one common approach used in clustering measurements is the nearest neighbor method (Zehavi et al. 2002, 2005, 2011; Berlind et al. 2006; Anderson et al. 2012). For fiber-collided galaxies without resolved redshifts, the method assigns the statistical weight of the fiber-collided galaxy to its nearest angular neighbor. This provides a reasonable correction for the fiber collision effects at scales much larger than the fiber collision scales; however the correction falls short elsewhere. In fact, as Zehavi et al. (2005) find, fiber collisions affect the two-point correlation function (2PCF) measurements even on scales significantly larger than the fiber collision scale ($> 1 \text{ Mpc}/h$).

For power spectrum measurements in BOSS, the nearest neighbor method has recently been supplemented with adjustments in the constant shot-noise term of the power spectrum estimator to correct for fiber collisions (Beutler et al. 2014; Gil-Marín et al. 2014, 2015, 2016a; Beutler et al. 2016; Grieb et al. 2016; Gil-Marín et al. 2016b). More specifically, methods like the one used in Gil-Marín et al. (2014) obtain the value of the shot-noise term from mock catalogs and thus rely entirely on their accuracy to correct for fiber collisions. This is concerning since, as we shall demonstrate in detail, fiber collisions depend systematically on the small-scale power spectrum, and mock catalogs used for large scale structure analyses are typically not based on high resolution N-body simulations. In addition, there is no way to validate and calibrate the shot-noise term independently for observations. A more reliable approach is to marginalize over the value of the shot-noise term, and this is the approach that has recently become more popular (Beutler et al. 2014; Gil-Marín et al. 2016a; Beutler et al. 2016; Grieb et al. 2016; Gil-Marín et al. 2016b). However, adjustments to the shot-noise term are limited to the power spectrum monopole, since higher order multipoles do not have a shot-noise term. However, as we shall discuss in detail below, *fiber collisions affect all multipoles in a k -dependent way*, not just adding a constant for the monopole power.

Guo et al. (2012), focusing on SDSS-III BOSS like samples, proposed a fiber collision correction method for the 2PCF that is able to reasonably correct for fiber collisions above and below the collision scale. Guo et al. (2012) estimates the total contribution of fiber-collided galaxies to the 2PCF by examining the pair statistics in overlapping tiling regions of the survey, where a smaller fraction of galaxies suffer from fiber collisions. Unfortunately, applying an analogous method in Fourier space proves to be more difficult. The Guo et al. (2012) method in Fourier space would involve measuring the power spectra for individual overlapping regions. Given the complex geometry of these regions, the systematic effect introduced by the window function makes measuring the power spectrum at larger scales intractable.

Meanwhile, galaxy redshift-space power spectrum models from perturbation theory continue to reliably model higher k in the weakly non-linear regime (Taruya et al. 2010; Sato & Matsubara 2011; Taruya et al. 2012; Okumura et al. 2012; Taruya et al. 2013, 2014; Beutler et al. 2014; Okumura et al. 2015; Beutler et al. 2016;

Grieb et al. 2016; Sanchez et al. 2016). Recent analyses of galaxy power spectrum multipoles (Zhao et al. 2013; Beutler et al. 2014; Gil-Marín et al. 2014, 2016a; Beutler et al. 2016; Grieb et al. 2016; Gil-Marín et al. 2016b) use scales up to $k_{\text{max}} = 0.15 - 0.2h/\text{Mpc}$ for BOSS galaxies, and this limit will for sure move towards smaller scales in upcoming analyses. As statistical errors decrease the importance of systematics due to fiber collisions plays an increasingly important role. The main goal of this paper is to quantify this systematic effect for the power spectrum multipoles and to provide ways to overcome it; for this purpose we develop two distinct approaches.

The first approach improves upon the nearest neighbor method by modeling the distribution of the line-of-sight displacement between resolved fiber collided galaxies to statistically reconstruct the clustering of fiber-collided galaxies. This uses information on resolved fiber collided galaxies that is available from the data themselves (e.g. in tiling overlap regions). The difficulty with this method is that it works statistically, i.e. we cannot reconstruct the *actual* galaxy by galaxy line of sight displacement due to collisions. As a result of this, while the method works very well to recover the true power spectrum monopole from fiber collided galaxy catalogs, it does not work sufficiently well for the power spectrum quadrupole which is far more sensitive to the precise structure of “fingers of god”.

The second approach addresses the shortcomings of the first one by modeling the effects of fiber collisions on the *predictions* instead of trying to undo their effect on the data before computing power spectrum statistics. It approximates the effect of fiber collisions on the 2PCF as a 2D top hat function. Then it derives the effect of fiber collisions on the galaxy power spectrum as a convolution of the true power spectrum with the top hat function. Therefore the theoretical predictions for the power spectrum are fiber collided and then can be compared directly to the observed fiber collided power spectrum in clustering analyses.

This paper is organized as follows. In Section 2, we briefly describe the simulated mock catalogs with realistic fiber collisions and the power spectrum estimator used throughout the paper. We then demonstrate the impact of fiber collisions on power spectrum measurements and how the nearest neighbor method does not adequately account for fiber collisions in Section 3.1. We present our two methods of accounting for fiber collisions along with the results for mock catalogs in Section 3.2 and Section 3.3, respectively. Finally in Section 4 we summarize our results and conclude.

2. FIBER-COLLIDED MOCK CATALOGS

For various purposes, such as characterizing the impact of the survey window function on statistics and estimating covariance matrices, simulated mock catalogs play a crucial role in interpreting clustering measurements of observed galaxies (Cole et al. 1998; Scoccimarro & Sheth 2002; Yan et al. 2004; Anderson et al. 2012; Manera et al. 2013; Monaco et al. 2013; Beutler et al. 2014; Gil-Marín et al. 2014; White et al. 2014; Manera et al. 2015; Tassev et al. 2015; Carretero et al. 2015; Howlett et al. 2015; Izard et al. 2016; Chuang et al. 2015; Kitaura et al. 2016; Munari et al. 2016; Sunayama et al. 2016). They also provide a means of understanding systematic

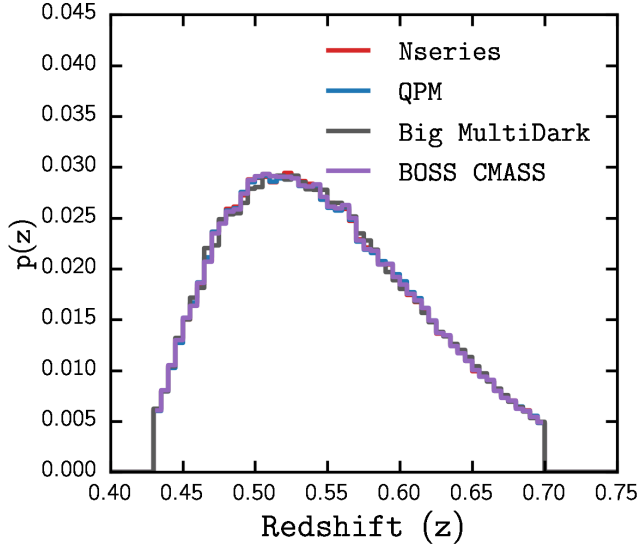


Figure 1. Normalized galaxy redshift distribution of the Nseries (orange), QPM (blue), and BigMultiDark (red) mock catalogs. The normalized redshift distribution of BOSS DR12 CMASS sample galaxies is also plotted (black). Each of the distributions were computed with a bin size of $\Delta z = 0.025$. All of the mock catalogs used in this work closely trace the BOSS CMASS redshift distribution.

effects such as fiber collisions (Guo et al. 2012; Manera et al. 2013). Since systematic effects can be simulated on them, they allow us to test how these effects influence clustering measurements and devise correction methods that attempt to account for these effects.

A direct way of understanding the effects of fiber collisions on clustering statistics in observations is to first apply fiber collisions to mock catalogs and then compare the clustering statistics obtained from mock catalogs with and without the fiber collisions. Correction methods for fiber collisions can then be applied to the fiber-collided mocks. The merit of the correction method can be assessed by how successfully they reproduce the clustering statistics of the original mock catalogs without fiber collisions. The correction method can then be applied to the observed data with some assurance that it accounts for fiber collisions and improves the clustering measurements.

When applying the fiber collisions to the mock catalogs, it is essential to apply them in the same manner they affect the observations. For BOSS, galaxies within $62''$ are fiber-collided (Anderson et al. 2012). In reality, this criteria is further complicated by the tiling scheme of observing plates that create overlapping regions, which have a higher success rate in resolving galaxy spectra within the fiber collision angular scale (Guo et al. 2012; Reid et al. 2012). Furthermore, fiber collisions are only one of the systematic effects that influence BOSS data. Systematic effects include the unique geometry of the BOSS survey, the variable completeness in different areas covered by unique sets of spectroscopic plates, and redshift failures (Anderson et al. 2012; Ross et al. 2012).

Effects of fiber collisions must be understood and interpreted in conjunction with the other systematic effects. Therefore, in this paper, we use Quick Particle Mesh (White et al. 2014), Nseries (Tinker et al. in prep), and

the BigMultiDark (Rodríguez-Torres et al. 2015) mock catalogs, which have already been extensively used in interpreting clustering results for BOSS and are generated through different prescriptions. Therefore they provide a robust sets of data to measure the effects of fiber collisions and to test our correction methods.

The QPM mock galaxy catalogs uses a “quick particle mesh” method, which uses a low resolution particle-mesh N-body solver, with a resolution of $2 \text{ Mpc}/h$, to evolve particles within a periodic simulation volume. The particles are assigned halo masses in order to match the halo mass function and large-scale bias of halos of high resolution simulations. Afterwards the HOD parameterization of Tinker et al. (2012) is used to populate the halos. The mock galaxy sample is then trimmed to the BOSS CMASS survey footprint, downsampled based on angular sky completeness (sector completeness) and radial selection. Furthermore, QPM mocks model the fiber collisions of the BOSS CMASS sample ($62''$). QPM uses the following Λ CDM cosmology: $\Omega_m = 0.29$, $\Omega_\Lambda = 0.71$, $\sigma_8 = 0.8$, $n_s = 0.97$ and $h = 0.7$. We use 100 realizations of the QPM catalog. For a detailed description of the QPM galaxy mock catalogs we refer readers to White et al. (2014).

Next, the Nseries mock catalogs are created from a series of high-resolution N-body simulations. Each mock has the same angular selection function as the North Galactic Cap region of the BOSS DR12 large-scale structure sample for CMASS galaxies (Cuesta et al. 2016). They also reproduce the redshift distribution of the BOSS CMASS sample. The Nseries mock catalogs are created from seven independent N-body simulations, each of the same cosmology. Each simulation box is $2.5 \text{ Gpc}/h$ per side with cosmology: $\Omega_m = 0.286$, $\Omega_\Lambda = 0.714$, $\sigma_8 = 0.82$, $n_s = 0.96$ and $h = 0.7$. Out of these Nseries box simulations, the three orthogonal projections of each box is used to create 84 mocks. Each of the cut-out mocks is then passed through the same fiber assignment code as the actual BOSS data using the distribution of plates in BOSS. Thus, the angular variation of fiber collisions faithfully reproduces that of the data, with $\sim 5\%$ of the targets without fibers due to close neighbors in regions of the footprint only covered by one tile.

Finally the BigMultiDark galaxy mock catalog is generated using the BigMultiDark Planck (BigMDPL), one of the MultiDark3 N-body simulations (Klypin et al. 2014). BigMDPL uses a GADGET-2 code (Springel 2005) in a cubic box of $2.5 h^{-1} \text{ Gpc}$ sides with 3840^3 dark matter particles and a mass resolution of $2.4 \times 10^{10} h^{-1} M_\odot$. As the name suggests, BigMDPL uses Planck cosmological parameters in a flat Λ CDM cosmology: $\Omega_m = 0.307$, $\Omega_B = 0.048$, $\Omega_\lambda = 0.693$, $\sigma_8 = 0.829$, $n_s = 0.96$ and $h = 0.678$.

From the BigMDPL N-body simulation, Rodríguez-Torres et al. (2015) uses the RockStar (Robust Over-density Calculation using K-Space Topologically Adaptive Refinement) halo finder (Behroozi et al. 2013) to obtain a dark matter halo catalog. Afterwards, they use the SURvey GenerAtor code (SUGAR) to generate a galaxy catalog from the halo catalog. SUGAR uses halo abundance matching with an intrinsic scatter on the stellar mass function of the Portsmouth SED-fit DR12 stellar mass catalog (Maraston et al. 2013) to populate the

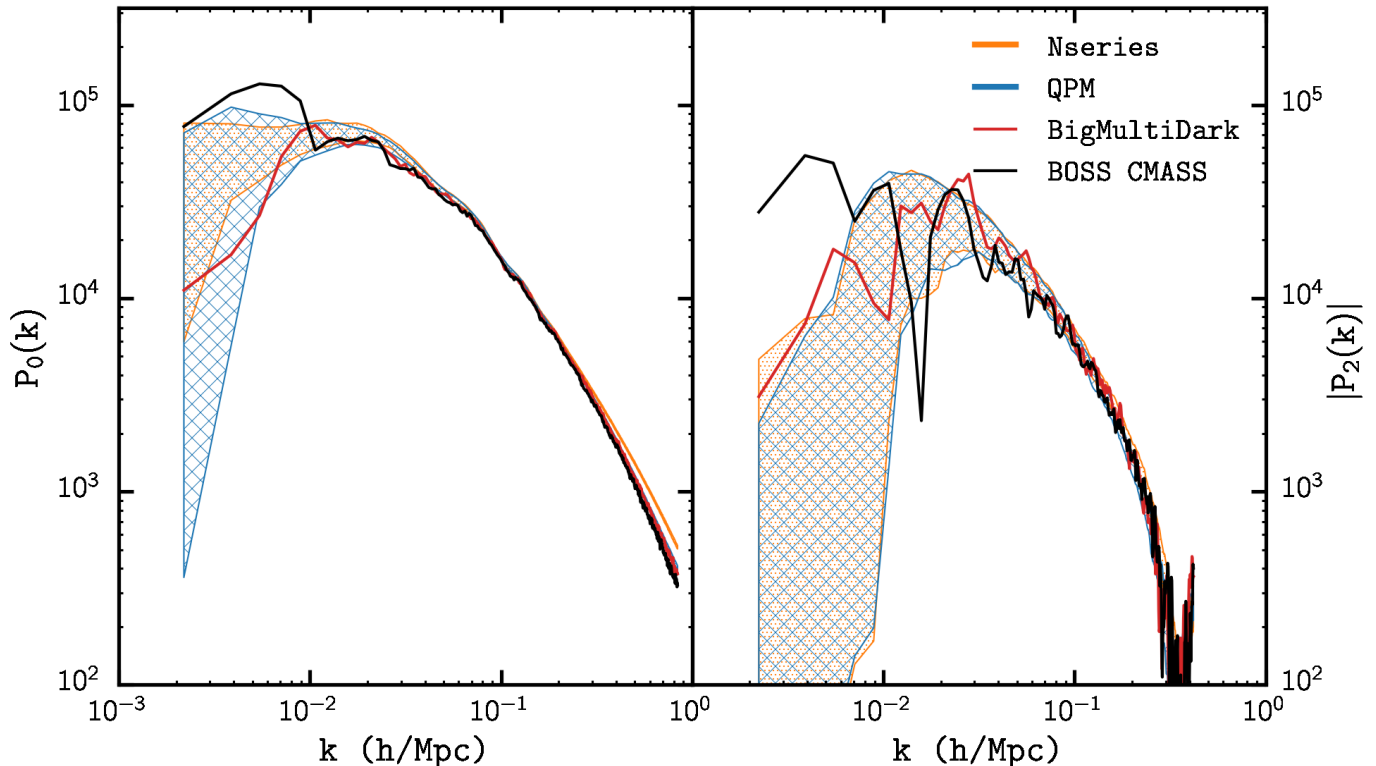


Figure 2. Power spectrum monopole $P_0(k)$ and quadrupole $|P_2(k)|$ measurements for the Nseries (orange), QPM (blue), and BigMultiDark (red) mock catalogs (Section 2). The $P_l(k)$ measurements for the Nseries and QPM mock catalogs are averaged over the multiple mock realizations and the width of the power spectra represents the sample variance ($\sigma_l(k)$; Eq. 10) of the realizations. For the quadrupole, we plot the $|P_2(k)|$ instead of $P_2(k)$ because the measurement becomes negative for $k \gtrsim 0.35 h/\text{Mpc}$. For comparison, we also include the monopole and quadrupole power spectra of the BOSS DR12 CMASS sample, which are calculated using the same estimator but with statistical weights described in Eq. (9). While fiber collisions are inevitably included in the BOSS CMASS power spectra, they are *not* yet applied to the mock catalogs power spectra measurements above.

dark matter halos with galaxies. Rodríguez-Torres et al. (2015) then model fiber collisions using Guo et al. (2012) in order to reproduce the effect of fiber collisions on the observed BOSS galaxies. For any further details on the BigMultiDark galaxy mock catalog, we refer readers to Rodríguez-Torres et al. (2015).

In Figure 1, we plot the normalized redshift distribution of the Nseries (orange), QPM (blue), and BigMultiDark (red) mock catalogs along with the redshift distribution of the BOSS DR12 CMASS sample galaxies. All of these mock catalogs were constructed for the BOSS analysis and their redshift distributions closely trace the observed BOSS distribution.

2.1. Power Spectrum Estimator

In this paper, out of the many possible clustering measurements, we focus on the galaxy power spectrum and its monopole and quadrupole in redshift space. Throughout the paper, unless specified, when we measure the power spectrum we use the estimator described in Scocimarro (2015), which accounts for radial redshift space distortions (see also Bianchi et al. 2016). In this estimator, galaxies are interpolated and Fast Fourier transformed as discussed in Sefusatti et al. (2016). Since the algorithm is efficient, it makes power spectrum computations for large number of mock realizations tractable.

To summarize the method, we calculate the monopole

component of the power spectrum using:

$$\widehat{P}_0(k) = \frac{1}{I_{22}} \left[\int \frac{d\Omega_k}{4\pi} |F_0(\mathbf{k})|^2 - N_0 \right] \quad (1)$$

where

$$F_0(\mathbf{k}) = \left(\sum_{j=1}^{N_g} -\alpha \sum_{j=1}^{N_r} \right) w_j e^{i\mathbf{k}\cdot\mathbf{x}_j} \quad (2)$$

with normalization constant

$$I_{22} = \alpha \sum_{j=1}^{N_r} \bar{n}(\mathbf{x}_j) w_j^2 \quad (3)$$

and shot noise term following from the estimator is (Scocimarro 2015)

$$N_0 = \left(\sum_{j=1}^{N_g} + \alpha^2 \sum_{j=1}^{N_r} \right) w_j^2, \quad (4)$$

which represents the constant shot noise contribution to the power due to the discrete density field of our galaxies and random catalog. Here α is the ratio of the number of galaxies (N_g) over the number of synthetic random galaxies (N_r), $\bar{n}(\mathbf{x})$ is the mean density of the galaxies at position \mathbf{x} , and w_j is weight of each object, which includes the minimum variance weight from Feldman et al.

(1994):

$$w_{\text{FKP}}(\mathbf{x}_j) = \frac{1}{1 + \bar{n}(\mathbf{x}_j)P_0} \quad (5)$$

where P_0 is the power spectrum amplitude at which the error is minimized. We use $P_0 = 20000 \text{ Mpc}^3/h^3$ for our analysis, which corresponds to $k \sim 0.1 h/\text{Mpc}$. We note that the shot noise term in Eq. (4) differs from the standard shot noise term from Feldman et al. (1994). The difference between various shot noise expressions used in the literature will be discussed in detail in Section 3.2.2.

For the quadrupole, we have

$$\widehat{P}_2(k) = \frac{5}{I_{22}} \int \frac{d\Omega_k}{4\pi} F_2(\mathbf{k}) F_0^*(\mathbf{k}) \quad (6)$$

where

$$F_2(\mathbf{k}) = \frac{3}{2} \hat{k}_a \hat{k}_b Q^{ab}(\mathbf{k}) - \frac{1}{2} F_0(\mathbf{k}) \quad (7)$$

with

$$Q^{ab}(\mathbf{k}) = \left(\sum_{j=1}^{N_g} -\alpha \sum_{j=1}^{N_r} \right) \hat{x}_j^a \hat{x}_j^b w_j e^{i\mathbf{k}\cdot\mathbf{x}_j} \quad (8)$$

In Figure 2, we plot the power spectrum monopole and quadrupole, $P_0(k)$ and $|P_2(k)|$, measured using Eq. (1) and Eq. (6), respectively, for the Nseries, QPM, and Big-MultiDark mock catalogs. We plot $|P_2(k)|$ because the power spectrum quadrupole becomes negative for $k \gtrsim 0.35 h/\text{Mpc}$. $P_0(k)$ and $|P_2(k)|$ are averaged over the 84 and 100 realizations for Nseries and QPM. We note that fiber collisions are not applied to these mock catalogs. Without fiber collisions, the weights of the objects are equivalent to the FKP weights, $w_j = w_{j,\text{FKP}}$.

We also plot the $P_0(k)$ and $P_2(k)$ of the BOSS Data Release 12 CMASS data (black) in Figure 2. For BOSS DR12 CMASS, systematic weights are assigned to the galaxies in order to account for sector completeness, redshift failures, and fiber collisions. Each galaxy has a statistical weight determined by,

$$w_{j,\text{tot}} = w_{j,\text{sys}}(w_{j,\text{rf}} + w_{j,\text{fc}} - 1), \quad (9)$$

(Anderson et al. 2012; Ross et al. 2012; Beutler et al. 2014), which are included in the final object weight w_j along with $w_{j,\text{FKP}}$. In this formula, $w_{j,\text{rf}}$ is a weight that accounts for redshift failures and $w_{j,\text{fc}}$ is the fiber collision weight determined by the nearest angular neighbor method, which we later discuss in Section 3.1. The statistical weights are also included in $\alpha = \sum_{j=1}^{N_g} w_{\text{tot}}/N_r$. We note that fiber collisions are inevitably included in the CMASS $P_l(k)$. However they are not yet included in the $P_l(k)$ of the mock catalogs in Figure 2.

For the mock catalogs with multiple realizations (QPM and Nseries), we compute the sample variance of the power spectrum

$$\sigma_l(k) = \sqrt{\frac{1}{N_{\text{mocks}} - 1} \sum_{i=1}^{N_{\text{mocks}}} (P_l^i(k) - \langle P_l(k) \rangle)^2}. \quad (10)$$

N_{mock} is the number of mock realizations (84 for Nseries and 100 for QPM) and $P_l^i(k)$ is the power spectrum for each realization. $\sigma_l(k)$ is represented in Figure 2 by the width of the shaded regions.

3. FIBER COLLISION METHODS

3.1. Nearest Angular Neighbor Method (NN)

A common approach to accounting for fiber collisions in clustering measurements has been to use the nearest angular neighbor method (Zehavi et al. 2002, 2005, 2011; Berlind et al. 2006; Anderson et al. 2012), hereafter NN method. For galaxies without resolved spectroscopic redshifts due to fiber collisions, the entire statistical weight of the galaxy is assigned to its nearest angular neighbor with resolved redshift. This method effectively assumes that all galaxies within the angular fiber collision scale ($< 62''$ for BOSS) are correlated with one another. In the context of the halo model, the NN method assumes that galaxies within the fiber collision angular scale reside in the same halo so displacing one of the galaxies and placing it on top of the other does not significantly impact clustering statistics. This is a reasonable assumption for the 2PCF and the power spectrum on scales far greater than fiber collisions.

One consequence of this method is that galaxies coincidentally within the angular fiber collision scale (hereafter referred to as ‘‘chance alignments’’) are incorrectly assumed to be gravitationally correlated and within the same halo. So when the statistical weight of the collided galaxy is added to its nearest angular neighbor, the collided galaxy is in fact displaced significantly from its true radial position. This displacement can even be on the scale of the survey depth, which corresponds to $\sim 500 \text{ Mpc}$ for BOSS. Furthermore, even for fiber collided galaxies that reside in the same gravitationally bound structures such as groups or clusters, up-weighting the nearest neighbor disregards the line-of-sight displacements within these structures.

To precisely quantify the effect of fiber collisions on the power spectrum, we compare the power spectrum measurements of the NN weighted fiber collided mock catalogs P_l^{NN} to the power spectrum measurements of the mock catalogs without fiber collisions, the ‘‘true’’ power spectrum P_l^{true} . Specifically, in Figure 3, we plot the power spectrum residual ($P_l^{\text{NN}} - P_l^{\text{true}}$) as a function of k . The power spectrum estimators Eq. (1) and (6) are used to calculate the monopole and quadrupole respectively. We include measurements of the sample variance, $\sigma_l(k)$, for the Nseries and QPM mock catalogs (Eq. 10). We also include the power spectrum residual $\Delta P_l^{\text{NoW}}(k) = P_l^{\text{NoW}}(k) - P_l^{\text{true}}(k)$ (dashed), where $P_l^{\text{NoW}}(k)$ is the power spectrum of the fiber collided mock catalogs with *no* NN weights, with the collided galaxies removed from the sample.

As both $P_l(k)$ and $\sigma_l(k)$ vary significantly over the probed k range, the significance of the discrepancies between $P_l^{\text{NN}}(k)$ and $P_l^{\text{true}}(k)$ are not adequately portrayed in Figure 3, especially for the monopole. Therefore, to compare P_0^{NN} and P_0^{true} over a wide k range and to especially highlight the discrepancies at small scales, in Figure 4, we compare the normalized monopole residuals, $1 - P_0^{\text{NN}}/P_0^{\text{true}}$, to the normalized sample variance, $\sigma_0(k)/P_0^{\text{true}}$.

For the monopole, Figure 3 demonstrates that while the NN method (circles) provides an overall improvement over applying no correction (crosses) at most scales, fiber collisions still significantly bias the corrected power spectrum at all scales. The effect also has a significant k dependence, which implies that an adjusted constant

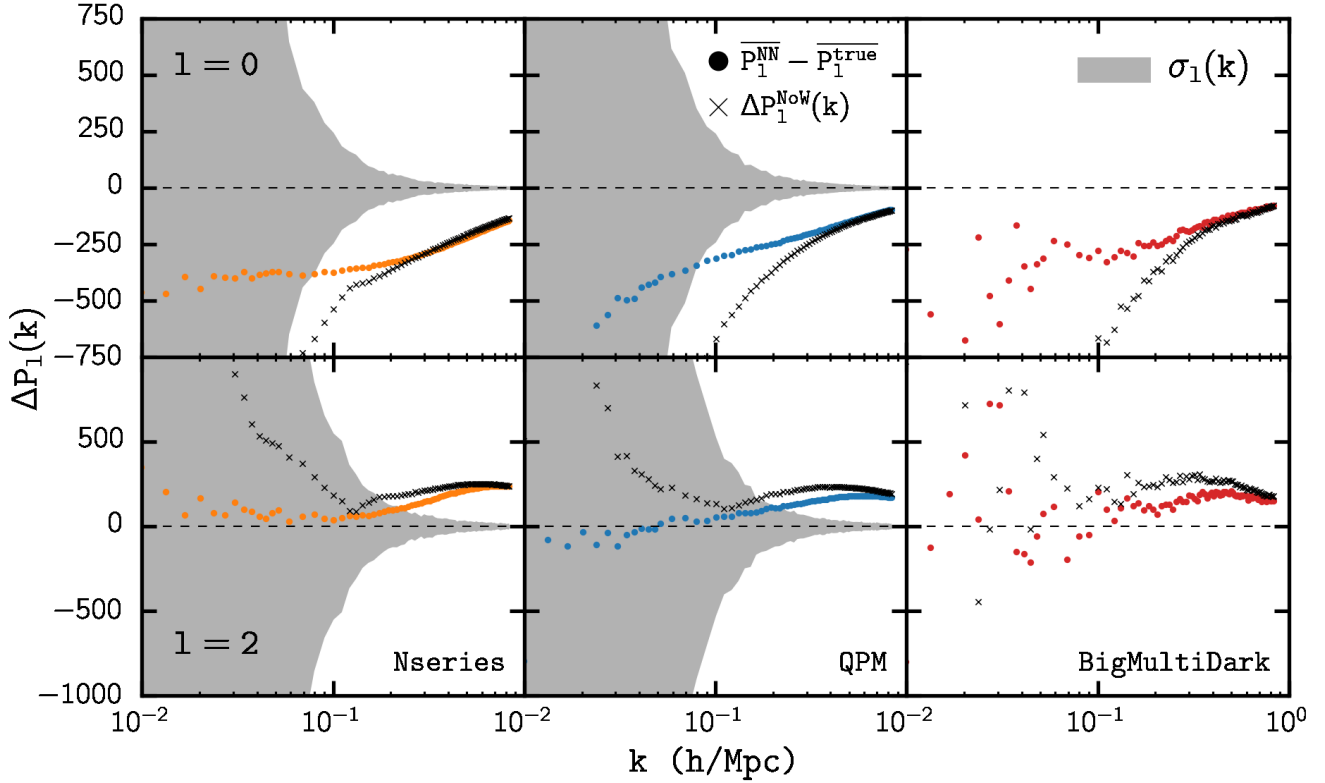


Figure 3. The fiber collision power spectrum residual, $(P_l^{\text{NN}} - P_l^{\text{true}})$ (Section 3.1), for the monopole (top) and quadrupole (bottom) of the Nseries (left), QPM (middle), and BigMultiDark (right) mock catalogs. For the Nseries and QPM mocks, we plot the sample variances $\sigma_l(k)$ (grey shaded region) of $P_l^{\text{true}}(k)$ for comparison. The power spectrum residual for the NN method is an improvement over the residual with no correction ($\Delta P_l^{\text{NoW}}(k)$; \times) at most scales probed. However, we highlight that at $k > 0.1 h/\text{Mpc}$ and $k > 0.2 h/\text{Mpc}$, for the monopole and quadrupole respectively, the residuals from fiber collision surpass the sample variance. At smaller scales, NN method does not sufficiently account for the effects of fiber collisions in $P_l(k)$ measurements.

shot noise term alone is insufficient in accounting for the deviation. Even at $k \approx 0.1 h/\text{Mpc}$, the effect of fiber collisions in the NN method alarmingly surpasses sample variance. While the amplitude of the residual decreases as k increases, Figure 4 reveals that as a fraction of $P_0^{\text{true}}(k)$, the discrepancy is in fact increasing. In other words, the NN method becomes less effective at correcting for fiber collisions on smaller scales, as expected. At the smallest scales probed ($k = 0.83 h/\text{Mpc}$), the $P_0^{\text{NN}}(k)$ underestimates the true power spectrum monopole by over 20%.

For the quadrupole, the NN method improves the power spectrum residuals over no correction. However, even with the NN method, the effect of fiber collisions begins to significantly grow at $k = 0.1 h/\text{Mpc}$ and becomes comparable to the sample variance at $k \sim 0.2 h/\text{Mpc}$. For $k > 0.2 h/\text{Mpc}$, the effect continues to increase and quickly overtakes the decreasing sample variance. At the smallest scales measured ($k = 0.83 h/\text{Mpc}$) the residual is over eight times the sample variance.

Recently power spectrum analyses have measured the power spectrum using a wide range of k bins: for example, Anderson et al. (2012) use $\Delta k = 0.04 h/\text{Mpc}$ and Beutler et al. (2014) and Grieb et al. (2016) use $\Delta k = 0.005 h/\text{Mpc}$. Here, we use $\Delta k = 0.01 h/\text{Mpc}$, which is within this general range, in agreement with Beutler et al. (2016) and Gil-Marín et al. (2016a). Sample variance measured with larger Δk is smaller; so a straight

comparison in Figure 3 between the power spectrum residuals (symbols) and the sample variance (shaded region) has a significant dependence on the choice of Δk . What is independent of binning is a cumulative χ^2 as a function of k , and thus we define a k scale limit k_{χ^2} so that $\Delta\chi^2(k_{\chi^2}) = 1$, where

$$\Delta\chi^2(k') = \sum_{i,j < N_k} [P_{l,i}^{\text{NN}} - P_{l,i}^{\text{true}}] C_{l,i,j}^{-1} [P_{l,j}^{\text{NN}} - P_{l,j}^{\text{true}}] \quad (11)$$

where N_k is the number of bins where $k < k'$ and $C_{l,i,j}^{-1}$ are the elements of the inverse covariance matrix for $P_l^{\text{true}}(k)$. The elements of the covariance matrix \mathbf{C}_l are computed as

$$C_{l,i,j} = \frac{1}{N_{\text{mocks}} - 1} \sum_{k=1}^{N_{\text{mocks}}} [P_{l,i}^{(k)} - \bar{P}_{l,i}] [P_{l,j}^{(k)} - \bar{P}_{l,j}]$$

for the Nseries and QPM mocks. For BigMD, which only has one realization, we use the covariance matrix of the Nseries realizations. In the lower panel of Figure 4, we mark the monopole and quadrupole $k_{\chi^2}^{\text{NN}}$ for the mock catalogs using the NN method. Arrows above the dashed line mark the monopole $k_{\chi^2}^{\text{NN}}$ for Nseries (orange), QPM (blue) and BigMultiDark (red) catalogs. Similarly, the arrows below the dashed line mark the quadrupole $k_{\chi^2}^{\text{NN}}$ for the mock catalogs. Averaged over the three mock catalogs, we get $k_{\chi^2}^{\text{NN}} = 0.068$ and $0.17 h/\text{Mpc}$ for the

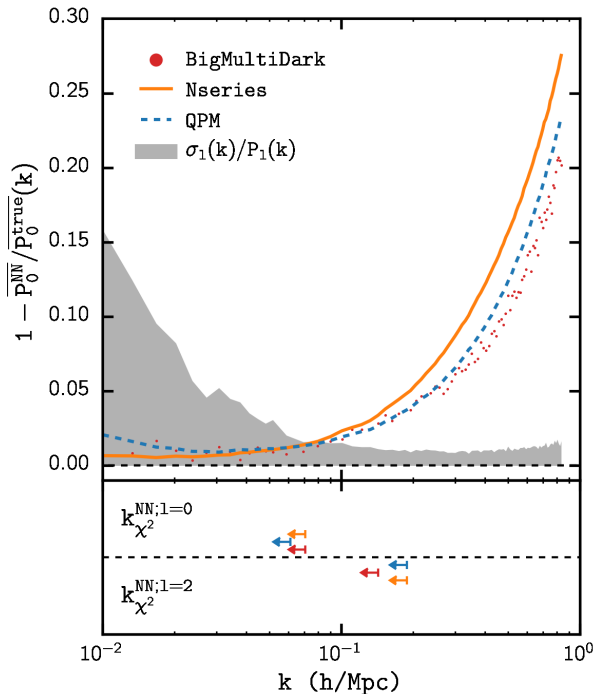


Figure 4. *Top Panel:* The normalized residuals, $1 - P_0^{\text{NN}}/P_0^{\text{true}}(k)$, of the NN method for the Nseries (orange), QPM (blue), and BigMultiDark (red) power spectrum monopole. We also plot the normalized sample variance $\sigma_0(k)/P_0(k)$ (gray shaded region) of the Nseries mocks for comparison. The QPM $\sigma_0(k)/P_0(k)$ is effectively the same as the Nseries $\sigma_0(k)/P_0(k)$, so we do not include in the figure. The comparison reveals that the effect of fiber collisions not only biases the power spectrum beyond sample variance at $k \gtrsim 0.1 h/\text{Mpc}$, but that the effect increases relative to sample variance at smaller scales. At $k = 0.2 h/\text{Mpc}$, the normalized residual is greater than 4 times the normalized sample variance.

Bottom Panel: We mark k_{χ^2} where $\Delta\chi^2(k_{\chi^2}) = 1$ (Eq. 11) for the NN method. $k_{\chi^2}^{\text{NN}}$ is a conservative scale limit of the NN method. Arrows above the dashed line mark k_{χ^2} for the monopole while the arrows below the dashed line mark k_{χ^2} for the quadrupole. The color of the arrows indicate the mock catalog: Nseries (orange), QPM (blue), and BigMultiDark (red). Averaged over the three mock catalogs, we get $k_{\chi^2}^{\text{NN}} = 0.068$ and $0.17 h/\text{Mpc}$ for the monopole and quadrupole respectively.

monopole and quadrupole respectively.

At $k = 0.2 h/\text{Mpc}$, the fiber collision residual for the monopole is over four times sample variance with average normalized residual of 4.4% compared to the 0.9% normalized sample variance. Moreover, we find that $k_{\chi^2} = 0.068 h/\text{Mpc}$, which is well below the maximum wavenumbers used typically in analyses. For the quadrupole, the fiber collision residual is approximately equivalent to sample variance at $k = 0.2 h/\text{Mpc}$ and $k_{\chi^2} = 0.17 h/\text{Mpc}$, but it quickly deteriorates with increasing k . Therefore for theoretical predictions that attempt to go beyond these scales, the effects of fiber collisions undoubtedly dominate the sample variance for both the power spectrum monopole and quadrupole and the NN method proves to be insufficient. In order to correct for this effect, we next present our first approach: the ‘line-of-sight reconstruction’ method.

3.2. Line-of-Sight Reconstruction Method

3.2.1. Line-of-Sight Displacement of Fiber Collided Pairs

It is impossible to determine definitively from observed galaxy data whether individual fiber collided galaxies without resolved spectroscopic redshifts are correlated or chance alignments. However, the line-of-sight displacement of fiber collided galaxy pairs with resolved redshifts make it possible to model the overall impact fiber collisions have on displacing galaxies.

For the BOSS galaxy catalog, fiber collided pairs with resolved spectroscopic redshifts are mainly located in the overlapping regions (Section 2). For the simulated mock catalogs, fiber collisions are post-processed after the galaxy positions are generated. Therefore, all galaxies in fiber collided pairs have resolved redshifts. From these resolved redshifts we calculate the comoving line-of-sight displacement (d_{LOS}) by taking the difference between the line-of-sight comoving distance of the resolved redshifts:

$$d_{\text{LOS}} = D_{\text{C}}(z_1) - D_{\text{C}}(z_2). \quad (12)$$

$D_{\text{C}}(z)$ here is the line-of-sight comoving distance at z (Hogg 1999), and z_1 and z_2 represent the resolved redshifts of the two galaxies in the fiber collided pair.

The normalized distributions of the calculated d_{LOS} for all resolved fiber collided pairs are presented in Figure 5 for Nseries (orange), QPM (blue), BigMultiDark (red), and BOSS DR12 (black). The d_{LOS} distributions for all catalogs consist of two components: a peak roughly within the range $-20 \text{ Mpc} < d_{\text{LOS}} < 20 \text{ Mpc}$ and a flat component (hereafter ‘tail’ component) outside the peak that extends to $d_{\text{LOS}} \sim \pm 500 \text{ Mpc}$. The entire range of the distribution is not displayed in Figure 5. For BOSS, as mentioned above, the d_{LOS} distribution only reflects the d_{LOS} values from galaxy pairs within the fiber collision angular scale with resolved spectroscopic redshifts, mostly from overlapping regions of the survey.

Galaxies within the same halo, due to their gravitational interactions at halo-scales, are more likely to be in close angular proximity with each other. These galaxies in over-dense regions cause the peak in the d_{LOS} distribution. The ‘tail’ component consists of chance aligned galaxy pairs that happen to be in close angular proximity in the sky.

Focusing on the peak of the distribution, we note that it closely traces a Gaussian functional form. Therefore, we fit

$$p(d_{\text{LOS}}) = A e^{-d_{\text{LOS}}^2/2\sigma_{\text{LOS}}^2} \quad (13)$$

for an analytic prescription of the d_{LOS} distribution peak as a function of d_{LOS} for each of the mock catalogs. We list the best-fit σ_{LOS} obtained by fitting Eq. (13) to the d_{LOS} distribution peak using MPFIT (Markwardt 2009) in Table 1. The parameter values in Table 1 and Figure 5 illustrate that the d_{LOS} distributions for the mock catalogs closely trace the BOSS DR12 distribution, which encourages our use of these mock catalogs in our investigation.

Using the best-fit to the peak of the d_{LOS} distribution, we estimate the fraction of collided pairs that are within the peak as the ratio of pairs with $|d_{\text{LOS}}| < 3\sigma_{\text{LOS}}$ over the total number of pairs:

$$f_{\text{peak}} = \frac{\sum_{|d_{\text{LOS}}| < 3\sigma_{\text{LOS}}} p(d_{\text{LOS}})}{N_{\text{pairs}}}, \quad (14)$$

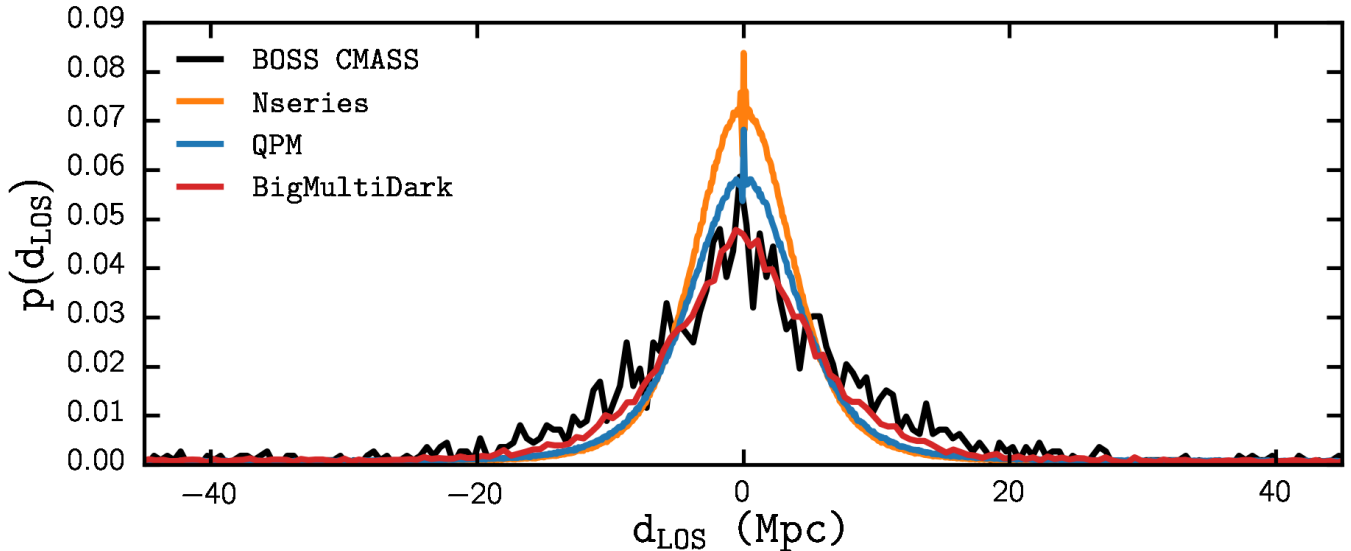


Figure 5. Normalized distribution of d_{LOS} for Nseries (orange), QPM (blue), and BigMultiDark (green) mock catalogs. The normalized d_{LOS} distribution of BOSS DR12 is also plotted (black). The mock catalog distributions have bin sizes of $\Delta d = 0.2$ Mpc, while the CMASS distribution has a bin size of $\Delta d = 0.5$ Mpc. The distribution extends beyond the range of the above plot to $\sim \pm 500$ Mpc. In the discussion of Section 3.2, we focus mainly on the peak of the distribution at roughly $-20 \text{ Mpc} < d_{\text{LOS}} < 20 \text{ Mpc}$.

Table 1
 d_{LOS} Distribution Best-fit Parameters

Catalog	σ_{LOS} (Mpc)	f_{peak}
Nseries	3.88	0.69
QPM	4.35	0.62
BigMultiDark	5.47	0.60
CMASS	6.56	0.70

Notes: Best-fit parameter σ_{LOS} (Eq. 13) and peak fraction f_{peak} (Eq. 14) for the d_{LOS} distributions in Figure 5.

where N_{pairs} is the total number of fiber collided pairs. f_{peak} roughly corresponds to the fraction of galaxy pairs that are correlated. The f_{peak} values calculated for the mock catalogs are listed in Table 1. They are consistent with the BOSS DR12 f_{peak} .

For the NN method of the previous section to be entirely correct, the d_{LOS} distribution in Figure 5 would have to be a delta function, which is clearly not the case. By simply incorporating the peak of the d_{LOS} distribution, we can significantly improve clustering statistics on small scales. Rather than placing the fiber collided galaxy on top of its nearest angular neighbor as the NN correction does, placing the fiber collided galaxy at a line-of-sight displacement, sampled from the peak of the d_{LOS} distribution, away from its nearest neighbor better reconstructs the galaxy clustering on small scales.

Only f_{peak} of the collided pairs should be displaced, since only f_{peak} of the fiber collided pairs are correlated. Meanwhile, the other $(1 - f_{\text{peak}})$ pairs should retain their NN weights since they are uncorrelated. Displacing these galaxies as well according to the tail piece of the d_{LOS}

distribution is not desirable because in an object by object basis we do not know which galaxies should actually be in the tail of the distribution, thus we will be making large mistakes in d_{LOS} galaxy by galaxy. In addition, it is difficult to incorporate that these galaxies should be correlated with others and ignoring this modifies large-scale power. In our approach, the remaining $(1 - f_{\text{peak}})$ fiber collided pairs are thus kept with their NN weights, and this is reflected in the shot noise correction of our estimator (Eq. 4), which in turn makes connection to previous methods in the literature as we now discuss.

3.2.2. Shot Noise Corrections

Measurements of the power spectrum are made on observations of discrete distributions of galaxies rather than continuous density fields. The discreteness contributes to the power spectrum. In order to correct for this contribution, galaxies are assumed to be Poisson samplings of the underlying distribution and a shot noise correction term is included in the power spectrum estimator (Peebles 1980; Feldman et al. 1994).

The expectation value of the shot noise term takes the following form (Feldman et al. 1994),

$$P_{\text{shot}} = \frac{(1 + \alpha) \int d^3r \bar{n}(\mathbf{r}) w^2(\mathbf{r})}{\int d^3r \bar{n}^2(\mathbf{r}) w^2(\mathbf{r})}. \quad (15)$$

Note that for the case of uniform weights ($w = \text{const.}$), constant number density and no random catalog this reduces to the standard shot-noise Poisson correction $P_{\text{shot}} = \bar{n}^{-1}$. In practice the integrals in Eq. (15) can be written as discrete sums over the synthetic random catalog (Feldman et al. 1994). $\int d^3r \bar{n}(\mathbf{r}) \dots$ is computed as $\alpha \sum_{\text{ran}} \dots$. Then the shot noise term becomes,

$$P_{\text{shot}}^{\text{FKP}} = \frac{(1 + \alpha) \alpha \sum_{\text{random}} w_{\text{FKP}}^2(\mathbf{r})}{\alpha \sum_{\text{random}} \bar{n}(\mathbf{r}) w_{\text{FKP}}^2(\mathbf{r})}. \quad (16)$$

This however, represents the expectation value of the shot noise, not the actual value (Hamilton 1997) since all quantities involved are mean values (calculated through the random catalog). To use the full information provided by the data, the shot noise of the galaxies should be computed from the actual galaxy weights, not the randoms. This simply corresponds to taking the self-pairs in the power spectrum estimator, Eq. (1), which leads to Eq. (4) and we can rewrite here as,

$$P_{\text{shot}}^{\text{Hahn+}} = \frac{\sum_{\text{galaxy}} w_{\text{FKP}}^2(\mathbf{r}) w_{\text{tot}}^2(\mathbf{r}) + \alpha^2 \sum_{\text{random}} w_{\text{FKP}}^2(\mathbf{r})}{\alpha \sum_{\text{random}} \bar{n}(\mathbf{r}) w_{\text{FKP}}^2(\mathbf{r})} \quad (17)$$

where $\alpha = (\sum_{\text{gal}} w_{\text{tot}})/N_r$. We emphasize that this is *the* shot noise of the estimator. In other words, if one takes the limit $k \rightarrow \infty$, the estimator in Eq. (1) will approach this value if no shot-noise subtraction is applied. The systematic effects from completeness, redshift failures and fiber collisions are accounted for through w_{tot} of the observed galaxies. In our case, $w_{\text{tot}} = w_{\text{sys}}$ for the resolved f_{peak} fraction of galaxies that have been displaced away from their NN positions, while $w_{\text{tot}} > w_{\text{sys}}$ for the $(1 - f_{\text{peak}})$ fraction of galaxies that are deemed to be in the tail of the LOS distribution and are described by NN weights of the galaxies they collided with.

Recent work in the literature of power spectrum analysis modeled the effect of fiber collisions by solely modifying the shot noise term for the NN method (Beutler et al. 2014; Gil-Marín et al. 2014). This assumes that the effect of fiber collisions beyond NN weights is to alter the large-scale effective shot noise, and therefore that only the power spectrum monopole is affected since the quadrupole is free of shot noise. Beutler et al. (2014) supplements the NN method with a shot noise correction term given by,

$$P_{\text{shot}}^{\text{B2014}} = \frac{\sum_{\text{galaxy}} w_{\text{FKP}}^2 w_{\text{tot}}(\mathbf{r}) w_{\text{sys}}(\mathbf{r}) + \alpha^2 \sum_{\text{random}} w_{\text{FKP}}^2(\mathbf{r})}{\alpha \sum_{\text{random}} \bar{n} w_{\text{FKP}}^2(\mathbf{r})}. \quad (18)$$

Note that in the first term of the numerator in this equation w_{fc} is only included in w_{tot} as it does not enter in w_{sys} . It is also worth noting that Beutler et al. (2014) ends up marginalizing over the value of the shot noise in their analysis, thus the impact of this particular choice is not straightforward.

Meanwhile, Gil-Marín et al. (2014) constructs P_{shot} using two separate components: one for “true pairs” and the other for “false pairs”. The shot-noise contribution to the power from “true pairs” is the same as Eq. (18) while the “false pairs” shot-noise contribution is (same as Eq. 17),

$$P_{\text{shot}}^{\text{False}} = \frac{\sum_{\text{galaxy}} w_{\text{FKP}}^2 w_{\text{tot}}^2(\mathbf{r}) + \alpha^2 \sum_{\text{random}} w_{\text{FKP}}^2(\mathbf{r})}{\alpha \sum_{\text{random}} \bar{n} w_{\text{FKP}}^2(\mathbf{r})}. \quad (19)$$

Gil-Marín et al. (2014) calculates the total P_{shot} as the

weighted combination of $P_{\text{shot}}^{\text{True}}$ and $P_{\text{shot}}^{\text{False}}$:

$$P_{\text{shot}}^{\text{GM2014}} = (1 - x_{\text{PS}}) P_{\text{shot}}^{\text{True}} + x_{\text{PS}} P_{\text{shot}}^{\text{False}} \quad (20)$$

In their analysis, Gil-Marín et al. (2014) use $x_{\text{PS}} = 0.58$, which they infer by measuring the difference between the true and the fiber-collided power spectrum monopole in the PTHalos galaxy mock catalogs (Manera et al. 2013). Unfortunately, since the true power spectrum is the measurement we are trying to recover from the observations, the x_{PS} parameter cannot be inferred or validated from the actual BOSS observations. Moreover, one might worry about relying PTHalos or similar methods that are not based on high resolution N-body simulations, to extract corrections for fiber collisions that depend on small-scale power. An extension of this approach is used in recent BOSS analyses (Beutler et al. 2016; Grieb et al. 2016; Gil-Marín et al. 2016b) where Eq. (20) is used and is supplemented with a marginalization over the shot noise value. However, as we discussed above, this has no effect in the quadrupole power spectrum, which remains the same as in the NN method.

At this point it is worth casting our “line-of-sight reconstruction” (LRec) method in similar language to the methods we just discussed. We treat the “true pairs” (what we called peak-pairs) by displacing them according to the peak LOS distribution, which modifies all the power spectrum multipoles, and use the NN method for the “false pairs” (pairs in the tail of the LOS distribution). Our shot noise correction is not adjusted, rather it is the true shot noise from the estimator. We now discuss the implementation and performance of our LRec fiber collision method.

3.2.3. In Practice

We first begin with fiber collided mock catalogs with the NN fiber collision weights that accurately simulate the effects of fiber collisions on the actual BOSS observations. From this catalog, we construct the d_{LOS} distribution, as described in Section 3.2.1 and fit for the best-fit parameters σ_{LOS} and f_{peak} of Eq. (13).

We select f_{peak} of the fiber collided galaxy pairs in the catalog and designate them as correlated pairs that lie within the peak of the d_{LOS} distribution. We refer to these fiber collided pairs as “peak-assigned”. At this point, each of these pairs, based on their NN weights, consist of the “nearest-neighbor” galaxy with $w_{\text{fc}} > 1$ and the “collided” galaxy with $w_{\text{fc}} = 0$. We discard the collided galaxy since the redshifts of collided galaxies are not known in actual observations.

Next for each of the nearest-neighbor galaxies in peak-assigned pairs, we place a new galaxy with $w_{\text{fc}} = 1$ at a displacement d_{peak} away from it along the line-of-sight but at the same angular position. The d_{peak} value is sampled from a Gaussian with best-fit σ_{LOS} from Table 1. The w_{fc} of the “nearest-neighbor” galaxy is then reduced by 1. This process is repeated, in the cases of triplets or higher with $w_{\text{fc}} > 2$, until all the nearest-neighbor galaxy in peak-assigned pairs have $w_{\text{fc}} = 1$. The resulting *total* catalog will have fewer galaxies with $w_{\text{fc}} > 1$ compared to the initial fiber collided catalog. However, the total statistical weight ($\sum_{\text{gal}} w_{\text{tot}}$) of the catalog, being equal to the total number of galaxies before the collisions are applied, is conserved.

Now that we have the “LOS reconstructed” mock

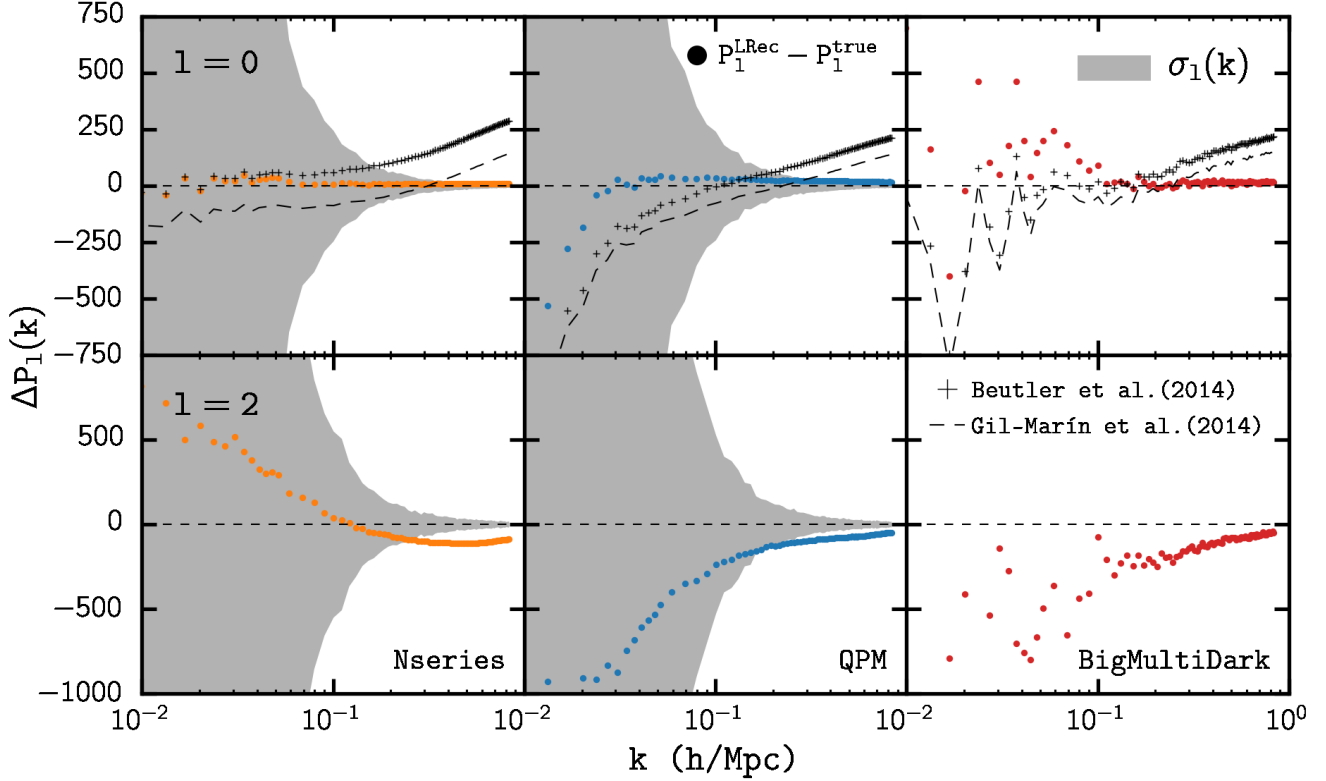


Figure 6. The power spectrum residual of the line-of-sight reconstruction (LRec) method (Section 3.2), $\Delta P_l \equiv P_l^{\text{LRec}} - P_l^{\text{true}}$, for the monopole (top) and quadrupole (bottom) power spectra of the Nseries (left), QPM (middle), and BigMultiDark (right) mock catalogs. We again plot the Nseries and QPM sample variances, $\sigma_l(k)$. The residuals for the monopole show good agreement between P_l^{LRec} and P_l^{true} for the entire k range. For the quadrupole, while the LOS Reconstruction method improves the residuals compared to the NN method at small scales ($k > 0.2 h/\text{Mpc}$), the residuals remain comparable to sample variance at $k = 0.2 h/\text{Mpc}$. In the top panels, we include the residuals from the fiber collision correction methods of Beutler et al. (2014) (plus) and Gil-Marín et al. (2014) (dashed). Both these corrections supplement the NN method with adjustments to the constant shot noise term of the estimator. As a result, they fail to correct for the k dependence of the effect and are insufficient in accounting for fiber collisions at small scales. Beutler et al. (2014) marginalizes over the correction in their analysis, so we plot the correction from Eq. (18) offset by -250 to match low- k residuals on the left panel.

catalog, we measure its power spectrum monopole and quadrupole (P_l^{LRec}). In Figure 6 we present the power spectrum residual, ($P_l^{\text{LRec}} - P_l^{\text{true}}$), for $l = 0$ and 2 of the LOS Reconstruction method power spectrum averaged over all the available realizations. We again include the Nseries and QPM sample variance, $\sigma_l(k)$ (grey shaded region) for comparison. In Figure 7, we normalize both the residuals and the sample variance by P_0^{true} to better compare P_0^{LRec} and P_0^{true} at different scales and to highlight the small scales.

For the monopole, at the scale where P_0^{NN} deviates from P_0^{true} by more than the sample variance ($k \sim 0.1 h/\text{Mpc}$), Figure 6 shows that the LOS reconstructed residual is well within the sample variance, $P_0^{\text{LRec}} - P_0^{\text{true}} < 0.17\sigma_0$. Even at the smallest scales measured for our monopole measurements ($k = 0.83 h/\text{Mpc}$), well beyond the scales that can be predicted from current models based on perturbation theory, the normalized residuals for the LOS reconstructed method remains at 3.7%. At $k \sim 0.2 h/\text{Mpc}$, the average normalized residual is 0.19% compared to the 0.9% normalized sample variance. When we calculate the k_{χ^2} of the LOS reconstruction method for the three mock catalogs, as we did for the NN method in Section 3.1, we get the average $k_{\chi^2}^{\text{LRec}} = 0.29 h/\text{Mpc}$ for the monopole. For each of the mocks, we mark $k_{\chi^2}^{\text{LRec}; l=0}$ in the lower panel of Figure 7

above the dashed horizontal line.

For the monopole, we also include the residuals from the fiber collision correction methods of Beutler et al. (2014) (pluses) and Gil-Marín et al. (2014) (dashed) in Figure 6. Both these analyses correct for fiber collisions by adjusting the constant shot noise term in the estimator in addition to the NN method (Section 3.2.2). However, as the NN method power spectrum residuals reveal in Figure 3, the effect has a k dependence, especially at $k > 0.1 h/\text{Mpc}$. So while these corrections can reduce the residuals to within sample variance at large scales, they fail to account for the k dependence, which quickly goes on to dominate sample variance at smaller scales, $k > 0.1 h/\text{Mpc}$.

We note that instead of using a fixed value for the constant shot noise as Gil-Marín et al. (2014) does, Beutler et al. (2014) marginalize over the constant term in their analysis. To reflect this, we offset the power spectrum residual we get using Eq. (18) by -250 in Figure 6 to force agreement at $k \rightarrow 0$ in the Nseries case. For simplicity, we only calculate k_{χ^2} for the Gil-Marín et al. (2014) correction method using the mock catalogs: $k_{\chi^2}^{\text{GM}+} = 0.17 h/\text{Mpc}$ (gray arrow; Figure 7), which is significantly lower than that of the LOS Reconstruction method. Compared to either method, the LOS reconstruction method better accounts for fiber collisions at all

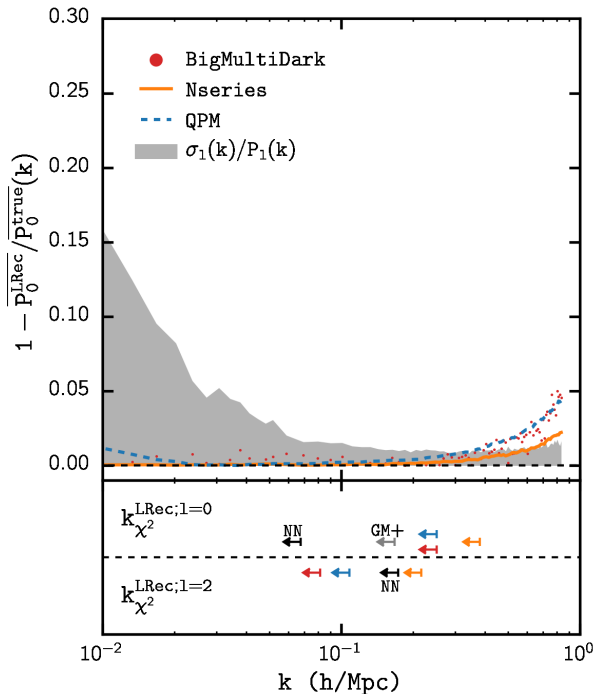


Figure 7. *Top Panel:* The normalized residual, $1 - P_0^{\text{LRec}}/P_0^{\text{true}}$, for the Nseries (orange), QPM (blue), and BigMultiDark (red) monopole power spectra. The normalized sample variance $\sigma_1/P_1(k)$ (gray shaded region) of the Nseries mocks is plotted for comparison. At $k = 0.1$ h/Mpc, where the NN method residuals exceeds sample variance, the average normalized residual for the LRec method is 0.25% compared to 1.5% normalized sample variance. In fact, the average residual stays below the sample variance until $k = 0.53$ h/Mpc.

Bottom Panel: We mark $k_{\chi^2}^{\text{LRec}}$ for the monopole (arrows above the dashed line) and quadrupole (arrows below the dashed line). The average $k_{\chi^2}^{\text{LRec}}$ for the mock catalogs are 0.29 and 0.14 h/Mpc for the monopole and quadrupole respectively. For comparison, we mark $k_{\chi^2}^{\text{NN}}$ (black) from Section 3.1. We also include k_{χ^2} of the Gil-Marín et al. (2014) correction method (gray) for the monopole. The LOS reconstruction method significantly extends k_{χ^2} beyond that of the NN method and Gil-Marín et al. (2014) for $l = 0$. However, it does not improve k_{χ^2} for the quadrupole.

scales. Furthermore, as already discussed the methods of Beutler et al. (2014) and Gil-Marín et al. (2014) do not provide corrections for the power spectrum quadrupole or higher multipoles, thus Figure 3 still applies for $l = 2$.

From Figure 6 we see that for the quadrupole, the LOS reconstruction method does not sufficiently improve corrections for fiber collisions compared to the NN method. The residuals for $k > 0.2$ h/Mpc are improved compared to Figure 3; however, they still exceed the sample variance. Unfortunately, these improvements on small scales come at the cost of increased residuals on large scales. In the k_{χ^2} marked in Figure 7 (below the dashed line), we see that the increased residuals at large scales actually make the average $k_{\chi^2}^{\text{NN}} > k_{\chi^2}^{\text{LRec}} = 0.14$ h/Mpc for the quadrupole, although there is significant dispersion between the different simulations with Nseries showing improvements when compared to the NN method while the other two showing worse performance. Consequently, neither the LOS reconstruction method nor the NN method sufficiently account for fiber collisions in the power spectrum quadrupole.

The shortcomings of the LOS reconstruction method

for the quadrupole compared to the monopole does not come as a surprise since the quadrupole is more sensitive to getting the correct LOS displacements galaxy by galaxy (not just statistically), as these modify the fingers-of-god effect. In order to make further progress with this method one would have to determine for each galaxy the most likely halo in which it lives (this could be nearby or a distant, chance alignment), determine its velocity dispersion and then assign a LOS displacement consistent with the dispersion and the observed LOS distribution.

Let us now discuss a few attempts that we have implemented along these lines. The first is incorporating more information about the fiber collided pairs in order to better classify correlated and chance alignment pairs. For example, information about larger scale galaxy environment in the form of the N^{th} nearest neighbor distance (d_{nNN}), can be included to parameterize the σ_{LOS} and f_{peak} (Table 1) as a function of d_{nNN} . The d_{nNN} in this case is the distance of the n^{th} nearest neighbor of the nearest-neighbor galaxy within the fiber collided pair. Another way the LOS reconstructed method can be improved is by utilizing the photometric redshifts of the collided galaxies to improve the correlated/change alignment pair classification.

We explored the LOS reconstructed method with both of these improvements on the mock catalogs. We find that there is indeed a significant correlation between d_{nNN} and the parameters σ_{LOS} and f_{peak} , which can be exploited. Also, photometric redshifts assigned to collided galaxies based on the $|z_{\text{spec}} - z_{\text{photo}}|/(1 + z_{\text{spec}})$ of actual BOSS photometric redshift catalogs improves classification of correlated versus chance alignment fiber collided pairs, as well. These improvements bring the normalized residuals of the monopole to $\sim 1\%$ at $k = 0.83$ h/Mpc. However, the improvement in the fiber collision correction for the quadrupole is marginal; the effect of fiber collisions at $k = 0.2$ h/Mpc is still comparable to the sample variance. So even with these improvements the LOS reconstructed method is insufficient.

Furthermore, for the Nseries mocks, we find that if we use the LOS reconstructed method with perfectly classified correlated and chance alignment pairs, the residual is roughly half the sample variance at $k \sim 0.2$ h/Mpc and greater than sample variance at $k > 0.35$ h/Mpc. The displacement of the collided galaxy by d_{LOS} sampled from Eq. (13) alone causes the power spectrum quadrupole to deviate from the true value at small scales. A method such as the LOS reconstructed method for the quadrupole would require more sophisticated modeling of the fiber collided galaxy pairs that capture the displacements in an object by object basis.

As a result of the shortcomings of the LOS reconstructed method for the power spectrum quadrupole, we now present a complementary approach in dealing with fiber collision in power spectrum multipole analyses, which rather than attempting to correct the data before making measurements, computes theoretical predictions of the fiber-collided power spectrum multipoles.

3.3. Effective Window Method

The LOS Reconstruction method corrects for fiber collisions in the observed galaxy positions in order to estimate the systematics-free true power spectrum. In power

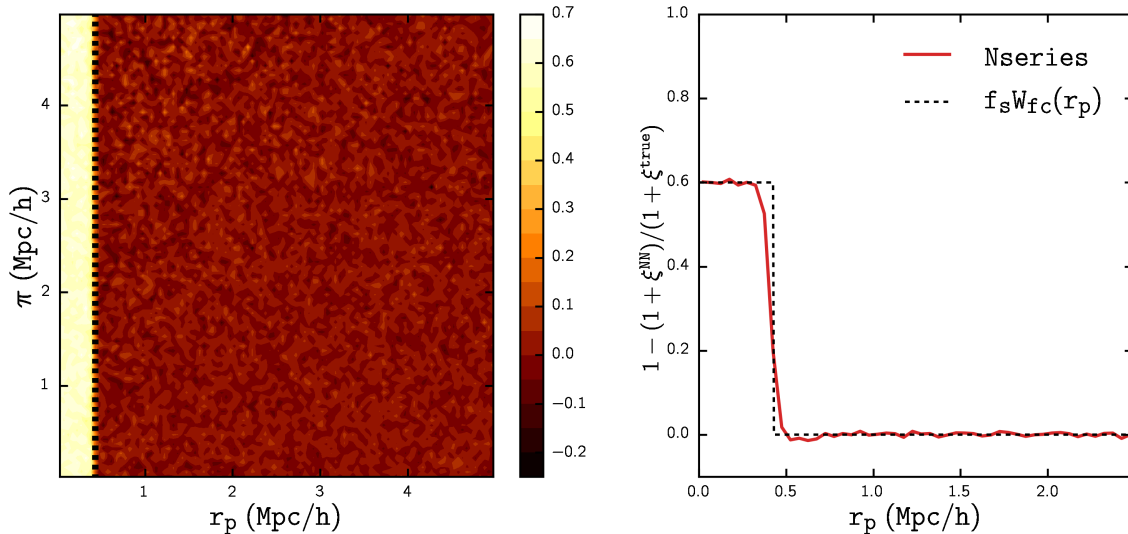


Figure 8. $1 - (1 + \xi^{\text{NN}})/(1 + \xi^{\text{true}})$ as a function of transverse displacement, r_p , and line-of-sight displacement π (left). The color bar represents the value of this quantity. Note there is no detectable dependence on π . The dashed vertical line (black) represents the constant $r_p = D_{\text{fc}}(z = 0.55)$ (Section 3.3). We also plot $1 - (1 + \xi^{\text{NN}})/(1 + \xi^{\text{true}})$ projected along π (right). In the left panel, the $r_p = D_{\text{fc}}(z = 0.55)$ vertical line and the sharp cut-off of the contour show good agreement with the expected characteristic scale. In the right panel, the projected $1 - (1 + \xi^{\text{NN}})/(1 + \xi^{\text{true}})$ is in good agreement with $f_s W_{\text{fc}}(r_p)$. The agreement in both panels justify the characterization of the effect of fiber collisions on the 2PCF in Eq. (21).

spectrum analyses, this true power spectrum estimate can be compared to model power spectrum for cosmological parameter inference. Alternatively, however, the observed fiber collided power spectrum can be compared to the model power spectrum with the effect of fiber collisions imposed on it. This is the approach we follow from now on.

We proceed as follows. In Section 3.3.1 we find that the effect of fiber collisions on the two-point correlation function can be well approximated by a simple analytic expression. Using this, we accurately estimate the effect of fiber collisions on the power spectrum in Fourier space. The effect is a function of the true power spectrum and depends significantly on the power spectrum at small scales, which cannot reliably be modeled from first principles. As a result, in Section 3.3.2, we present a practical approach to circumvent this issue and account for the effect of fiber collisions in power spectrum analyses.

3.3.1. In Theory

In the BOSS galaxy catalog, which spans the redshifts $0.43 < z < 0.7$, the comoving distance of the $62''$ fiber collision angular scale (D_{fc}) ranges from 0.35 Mpc to 0.52 Mpc. Given the relatively small variation in D_{fc} , we assume that throughout the survey redshift the physical scale remains constant as $D_{\text{fc}}(z \sim 0.55) = 0.43 \text{Mpc}$, at the median redshift of the survey. If the physical scale of fiber collisions is constant, fiber collisions will affect the two-dimensional configuration space two-point correlation function, $\xi(r_p, \pi)$, through its effect on galaxy pairs with transverse separations $r_p < D_{\text{fc}}$. As no pairs will be found below this characteristic scale, $\xi(r_p, \pi)$ will be -1 for $r_p < D_{\text{fc}}$, and note that the same is true for the two-point function in the NN method (since small- r_p pairs are collapsed into zero separation described by weights). On the other hand, at large scales we can ap-

proximate $\xi(r_p, \pi)$ by the NN method which preserves the large-scale angular correlation function, thus the effect of fiber collisions on $\xi(r_p, \pi)$ can be analytically characterized by the following relation between the true and the NN two-point functions,

$$\frac{1 + \xi^{\text{NN}}(r_p, \pi)}{1 + \xi^{\text{true}}(r_p, \pi)} = 1 - f_s W_{\text{fc}}(r_p) \quad (21)$$

where $W_{\text{fc}}(r_p)$ represents the top-hat function

$$W_{\text{fc}}(r_p) = \begin{cases} 1 & \text{if } r_p < D_{\text{fc}} \\ 0 & \text{otherwise} \end{cases} \quad (22)$$

and f_s represents the fraction of the survey area affected by fiber collisions. Note in Eq. (21) we have assumed that we can linearly superpose the contributions to the two-point function from regions with and without collisions, and a key property of Eq. (21) is that its right hand side does not depend on π , something we test explicitly below. In the BOSS, f_s is precisely known because it corresponds to the fraction of the survey geometry that suffers from fiber collisions. These are the regions that do not have overlapped tiling (Section 2). For BOSS DR12 $f_s = 0.6$.

We measure ξ^{NN} and ξ^{true} for the Nseries mock catalogs using the CUTE software (Alonso 2012), which uses the standard Landy & Szalay (1993) estimator. ξ^{NN} is calculated from the NN fiber collided Nseries mocks while ξ^{true} is calculated from the Nseries mocks without fiber collisions. Using the measured ξ^{NN} and ξ^{true} , we plot $1 - (1 + \xi^{\text{NN}})/(1 + \xi^{\text{true}})$ averaged over realizations as a function of r_p and π (left) and its projection along π (right) in Figure 8. The dashed vertical line (black; left) marking $r_p = D_{\text{fc}}(z = 0.55)$ and $f_s W_{\text{fc}}(r_p)$ (black dashed; right) are plotted for compar-

ison. The agreement between the $\xi(r_p, \pi)$ contours and the $r_p = D_{\text{fc}}(z = 0.55)$ cutoff along with the agreement between the projection and $f_s W_{\text{fc}}(r_p)$ justify our assumption of a constant physical fiber collision scale. The exact survey tiling of the BOSS sample is imposed on the Nseries mocks, so we expect Figure 8 to hold for the BOSS observations. The left panel illustrates the π -independence of the left hand side of Eq. (21). The right panel demonstrates that $1 - (1 + \xi^{\text{NN}})/(1 + \xi^{\text{true}})$ projected along π agrees remarkably well with a top-hat function.

In principle, however, W_{fc} is not necessarily a top-hat function. In fact, in eBOSS, due to the complex targeting scheme involving “knock-outs” from higher priority targeting samples, W_{fc} will not be top-hat function (Zhai et al. in prep). However, these complications are not present in our implementation of collisions; the reason for the deviations from a top-hat function here can be thought as arising from a sum of top-hats of slightly different radii along the line of sight (for fixed angular scale) weighted by the probability of collisions at each depth, leading to a smoother transition than a sharp top-hat function. In principle, our formalism can be improved by including this numerical profile rather than a top-hat, as we shall mention below (see discussion after Eq. 34).

With the confirmation of Eq. (21), we solve for ξ^{NN} :

$$\xi^{\text{NN}}(r_p, \pi) = \xi^{\text{true}}(r_p, \pi) - f_s W_{\text{fc}}(r_p) (1 + \xi^{\text{true}}(r_p, \pi)), \quad (23)$$

and to get an expression for the power spectrum, we Fourier transform to get

$$\begin{aligned} \Delta P(\mathbf{k}) &\equiv P^{\text{NN}}(\mathbf{k}) - P^{\text{true}}(\mathbf{k}) \\ &= -f_s W_{\text{fc}}(\mathbf{k}) - f_s \int \frac{d^3 q}{(2\pi)^3} P(\mathbf{q}) W_{\text{fc}}(\mathbf{k} - \mathbf{q}). \end{aligned} \quad (24)$$

We see that the effect of fiber collisions on the true power spectrum can be characterized by two terms: Fourier transform of the top-hat function (corresponding to chance collisions) and the power spectrum convolved with the top-hat function (corresponding to physically correlated pairs). We refer to these two terms as ΔP^{uncorr} and ΔP^{corr} respectively. Note that none of these terms is independent of k .

The first term, ΔP^{uncorr} , can be easily obtained:

$$\begin{aligned} \Delta P^{\text{uncorr}} &= -f_s \widehat{W_{\text{fc}}}(\mathbf{k}) = -f_s \int e^{i\mathbf{k}\cdot\mathbf{r}} W_{\text{fc}}(\mathbf{r}) d^3 r \\ &= -f_s 2\pi \delta_D(k_{\parallel}) \pi D_{\text{fc}}^2 W_{2\text{D}}(k_{\perp} D_{\text{fc}}). \end{aligned} \quad (25)$$

where $W_{2\text{D}}(x) \equiv 2J_1(x)/x$ is the top-hat function in 2D (a cylinder), and J_1 is a Bessel function of the first kind and of order 1. The multipole contributions of Eq. (25) are then

$$\Delta P_l^{\text{uncorr}}(k) = -f_s (2l+1) \mathcal{L}_l(0) \frac{(\pi D_{\text{fc}})^2}{k} W_{2\text{D}}(k D_{\text{fc}}), \quad (26)$$

where \mathcal{L}_l are the Legendre polynomials. The k^{-1} prefactor here, arising from the delta function in Eq. (25) is an approximation for scales smaller than the survey size, since the delta function follows from assuming we can integrate up to infinity along the line of sight in Eq. (25).

Equation (26) gives a correction that alternates in sign as a function of multipole l . Note that since for practical purposes $k D_{\text{fc}} \ll 1$, we can expand

$$\begin{aligned} \Delta P_l^{\text{uncorr}}(k) &= -f_s \pi D_{\text{fc}}^2 \left(\frac{2\pi}{k}\right) \frac{(2l+1)}{2} \mathcal{L}_l(0) \\ &\quad \times \left(1 - \frac{(k D_{\text{fc}})^2}{8} + \dots\right), \end{aligned} \quad (27)$$

and for scales involved in typical analysis the first term suffices, which means that the uncorrelated piece of fiber collisions decays as k^{-1} across the relevant range of scales. The magnitude of this uncorrelated effect (chance collisions) is small, given by the effective survey area affected by fiber collisions $f_s \pi D_{\text{fc}}^2$ times the wavelength of perturbations $2\pi/k$.

For the correlated piece ΔP^{corr} , we see from Eqs. (24) and (25) that we need $W_{2\text{D}}(|\mathbf{k}_{\perp} - \mathbf{q}_{\perp}| D_{\text{fc}})$ for which we can use the addition theorem for 2D top-hat functions (?),

$$\begin{aligned} W_{2\text{D}}(|\mathbf{k}_{\perp} - \mathbf{q}_{\perp}| D_{\text{fc}}) &= \sum_{k=0}^{\infty} (k+1) U_k(\hat{k}_{\perp} \cdot \hat{q}_{\perp}) \\ &\quad W_{2\text{D}}^{(k/2)}(k_{\perp} D_{\text{fc}}) W_{2\text{D}}^{(k/2)}(q_{\perp} D_{\text{fc}}) \end{aligned} \quad (28)$$

where the U_k 's are the Chebyshev polynomials and $W_{2\text{D}}^{(k/2)}(x) \equiv 2J_{k+1}(x)/x$. Now, again, as we are interested in scales for which $k D_{\text{fc}} \ll 1$ is an excellent approximation, dropping $\mathcal{O}(k_{\perp} D_{\text{fc}})^2$ we can just use the $k=0$ term in this expression. This gives us $W_{2\text{D}}(|\mathbf{k}_{\perp} - \mathbf{q}_{\perp}| D_{\text{fc}}) \approx W_{2\text{D}}(q_{\perp} D_{\text{fc}})$ as expected and leads to,

$$\Delta P^{\text{corr}}(\mathbf{k}) \approx -f_s \pi D_{\text{fc}}^2 \int \frac{d^2 q_{\perp}}{(2\pi)^2} P(k_{\parallel}, q_{\perp}) W_{2\text{D}}(q_{\perp} D_{\text{fc}}) \quad (29)$$

This is a simple result, showing that the correlated effect of fiber collisions is proportional to the effective survey area affected by fiber collisions and to the integral of the power spectrum over 2D modes perpendicular to the line of sight smoothed at the fiber collision scale. The multipole components of Eq. (29) are, after expanding $P(k_{\parallel}, q_{\perp})$ in multipoles,

$$\Delta P_l^{\text{corr}}(k) \approx -\frac{f_s D_{\text{fc}}^2}{2} \sum_{l'=0}^{\infty} \int_0^{\infty} dq q P_{l'}(q) f_{ll'}(k, q), \quad (30)$$

where, again neglecting $\mathcal{O}(k D_{\text{fc}})^2$,

$$\begin{aligned} f_{ll'}(k, q) &\equiv \left(\frac{2l+1}{2}\right) \int_{\max(-1, -q/k)}^{\min(1, q/k)} d\mu \mathcal{L}_l(\mu) \mathcal{L}_{l'}(k\mu/q) \\ &\quad \times W_{2\text{D}}(q D_{\text{fc}}) \end{aligned} \quad (31)$$

This has a simple expression for $l=l'$,

$$f_{ll}(k, q) = f_*(k, q) W_{2\text{D}}(q D_{\text{fc}}) \left(\frac{k_{<}}{k_{>}}\right)^l \quad (32)$$

where $f_*(k, q) = q/k$ for $q \leq k$ and unity otherwise, and $k_{>} = \max(k, q)$ and $k_{<} = \min(k, q)$. On the other hand,

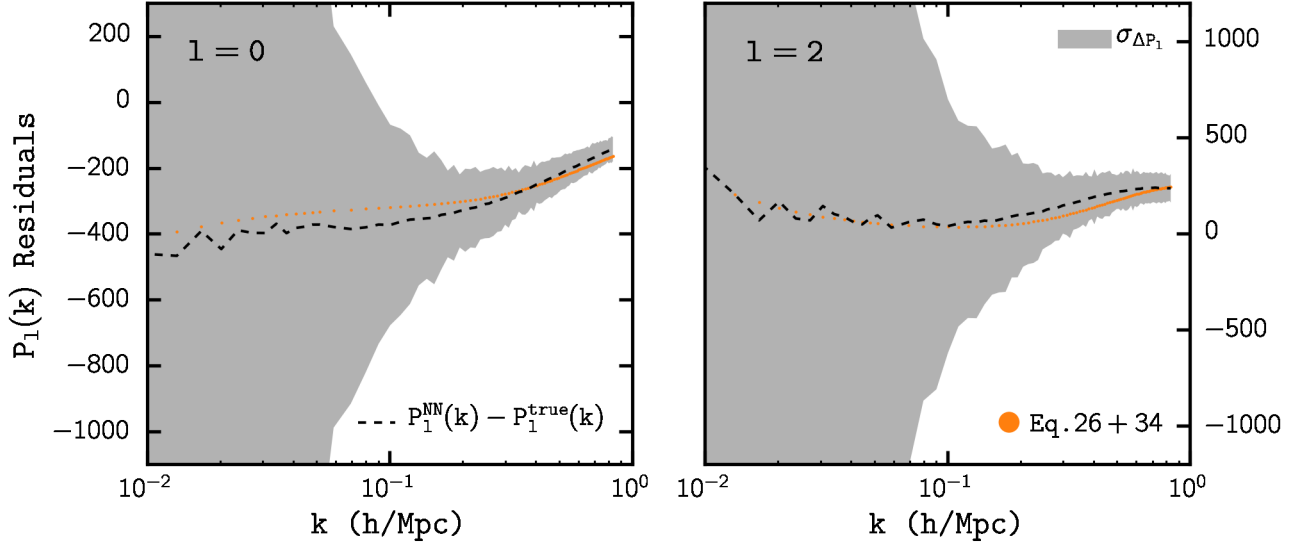


Figure 9. Comparison of the power spectrum residuals from NN-corrected fiber collisions $\Delta P_l = P_l^{\text{NN}} - P_l^{\text{true}}$ (dashed black) with the ΔP_l from the effective window method obtained by adding Eqs. (26) and (34) (orange) for the monopole (left) and quadrupole (right). The standard deviation of the power spectrum residual, $\sigma_{\Delta P_l}$, for the Nseries mock catalogs is shaded in gray.

off the diagonal we have ($l \neq l'$)

$$f_{l'l}(k, q) = f_*(k, q) W_{2D}(q D_{\text{fc}}) \left(\frac{2l+1}{2} \right) H_{l_>l_<} \left(\frac{k_<}{k_>} \right), \quad (33)$$

where $l_> = \max(l, l')$ and similarly $l_<$, and $H_{l_>l_<}(x)$ is a polynomial of degree $l_>$ which vanishes unless l and k are both larger or smaller than l' and q respectively. The first few polynomials are listed in the Appendix. Since $f_{l_>l_<}(k < q) = f_{l_<l_>}(k > q) = 0$ it is convenient to split the integrals depending on whether q is larger or smaller than k , which leads to

$$\Delta P_l^{\text{corr}}(k) \approx -\frac{f_s D_{\text{fc}}^2}{2} \left[\sum_{l' \leq l} \int_0^k q dq P_{l'}(q) f_{l'l}(q \leq k) + \sum_{l' \geq l} \int_k^\infty q dq P_{l'}(q) f_{l'l}(q \geq k) \right], \quad (34)$$

which shows that the change of power spectrum multipole l due to correlated fiber collisions comes from long modes of lower multipoles ($l' \leq l$) and short modes of higher multipoles ($l' \geq l$). Going back to the results displayed in Figure 8, we can now formulate how our results change if we use the observed numerical profile in the right panel of Figure 8 (red line) instead of the top-hat (black dashed). One can check that to leading order in $k D_{\text{fc}}$, which is all we are using in this paper, our expression for the uncorrelated and correlated change in power are valid as long as we replace the 2D top-hat by the numerical profile in Eq. (31), and redefine the scale D_{fc} that appears in Eqs. (27) and (30) from the area of the numerical profile, that is

$$\int d^2 r_\perp W_{2D}(\mathbf{r}_\perp) \equiv \pi D_{\text{fc}}^2 \quad (35)$$

We now proceed to testing these results, for which we need the true power spectrum multipoles down to small scales to feed into Eq. (34). Unfortunately, in the nonlinear regime the multipole expansion is not very efficient

(in the sense that the amplitude of multipoles does not decrease sharply with increasing multipole), so a large number of multipoles l' is required to capture the contribution from small scale modes. Measuring multipoles higher than the hexadecapole for realistic survey geometries using our estimator becomes expensive due to the number of Fast Fourier Transforms (FFTs) that needs to be computed, and even for the most efficient version of the multipole estimators that requires only 7 FFTs one would worry about increased cosmic variance (see discussion in Scoccimarro 2015).

A more efficient approach is to use the Nseries simulation boxes to test Eqs. (25) and (34). The Nseries simulation boxes are the original simulations where the Nseries mocks were cut out from (Section 2). Since the Nseries mocks are cut outs of the boxes, discrepancies in their power spectra are caused by the BOSS survey geometry and occur mainly at the largest scales, $k < 0.05 h/\text{Mpc}$ (Beutler et al. 2014; Grieb et al. 2016). At smaller scales, the difference between the power spectrum monopole, quadrupole and hexadecapole of Nseries mocks versus the Nseries boxes are negligible. Therefore, we calculate the $P_{l'}(q)$ from the Nseries simulation box, using periodic boundary conditions, which only requires one FFT and go up to $q = 43.5 h/\text{Mpc}$ and $l' = 18$ to compute the corrections predicted by Eq. (34).

In Figure 9, we compare $\Delta P_l = \Delta P_l^{\text{corr}} + \Delta P_l^{\text{uncorr}}$ calculated from the Nseries Box power spectrum multipoles using Eqs. (25) and (34) (orange) to the Nseries mock catalogs power spectrum residuals, $\Delta P_l = P_l^{\text{NN}} - P_l^{\text{true}}$ (dashed). The left panel compares the monopoles ($l = 0$) while the right panel compares the quadrupoles ($l = 2$). We also include in the gray shaded region, the standard deviation of Nseries mock catalogs power spectrum residuals, $\sigma_{\Delta P_l}$. For both the monopole and quadrupole, the predictions (orange) agree with the measured residuals from NN-corrected fiber collisions (dashed black) well within the errors throughout the probed k range up to $k = 0.83 h/\text{Mpc}$. At low- k , the downturn (upturn) in

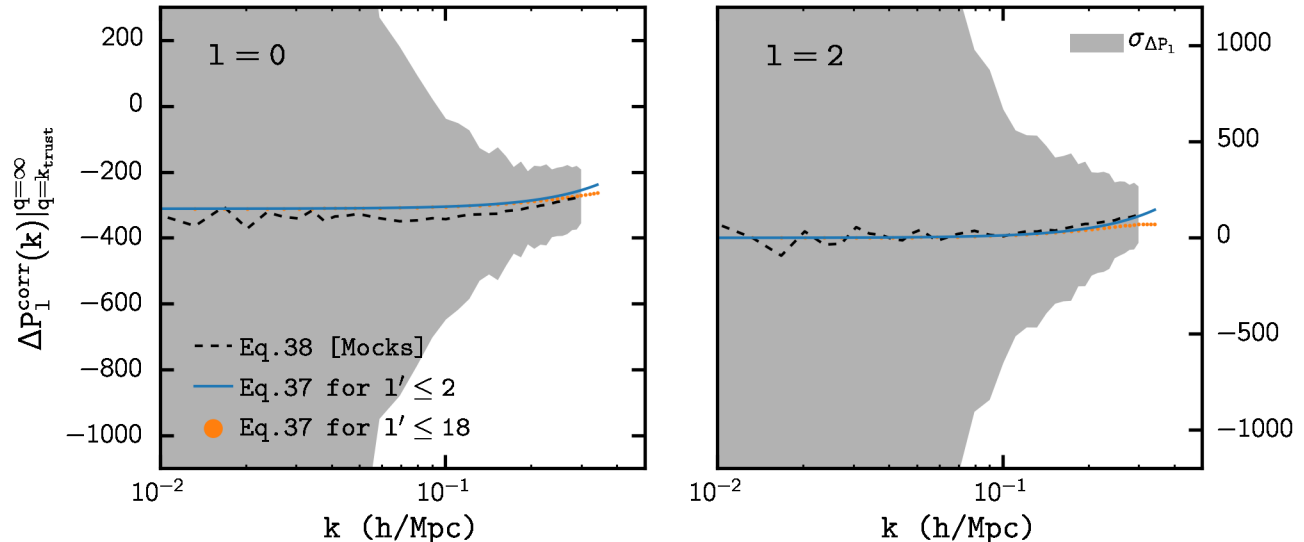


Figure 10. Comparison of the correlated power spectrum residuals from unreliable modes obtained from mocks (dashed), Eq. (38), to the polynomial approximation of Eq. (37) for $l' \leq 18$ (orange). The left and right panels correspond to $l = 0$ and 2 respectively. The gray shaded region is the standard deviation for the Nseries ($P_l^{\text{NN}} - P_l^{\text{true}}$). We also include Eq. (37) evaluated only for $l' \leq 2$ (blue). The agreement between Eq. (37) for $l' \leq 2$ and Eq. (38) demonstrate that while higher orders of l' are necessary to properly model $\Delta P_l^{\text{corr}}(k)$ at higher k values, for $k < k_{\text{trust}}$ ($0.3 h/\text{Mpc}$ above) $l' \leq 2$ are sufficient.

the monopole (quadrupole) is due to the contribution of the k^{-1} uncorrelated piece. The overall quality of the agreement demonstrates that the effective window method can be used to robustly estimate the effect of fiber collisions on $P_l(k)$. Furthermore, with its excellent performance for the quadrupole, the effective window approach provides an improvement over the LOS reconstruction method (Section 3.2).

3.3.2. In Practice

There are, however, practical limitations to the effective window model as it described above. The ΔP_l^{corr} calculations in Eq. (34) involves integrating the power spectrum over the q range of 0 to ∞ . While this integral converges for $q \approx 10 h/\text{Mpc}$ for both monopole and quadrupole, in practice one cannot compute reliably the power spectrum multipoles down to these scales. We now discuss a way to overcome this issue.

Let k_{trust} represent the scale up to which we can calculate reliably power spectrum multipoles. We therefore split the second term in Eq. (34) into a reliable piece (integration from k to k_{trust}) and an unreliable piece (integration from k_{trust} to ∞), so schematically

$$\Delta P_l^{\text{corr}} = \Delta P_l^{\text{corr}} \Big|_{q=0}^{q=k_{\text{trust}}} + \Delta P_l^{\text{corr}} \Big|_{q=k_{\text{trust}}}^{q=\infty}. \quad (36)$$

The first term can be reliably calculated from first principles since it involves modes from $q = 0$ to $q = k_{\text{trust}}$ and corresponds to the first term plus the reliable piece of the second term in Eq. (34). Now, the key fact is that because the second term in Eq. (36) only depends on k through $f_{l\nu}(q \geq k)$, from Eqs. (32-33) it follows that the k -dependence of the unreliable term is simply a polynomial in k ,

$$\Delta P_l^{\text{corr}} \Big|_{q=k_{\text{trust}}}^{q=\infty} = \sum_{n=0,2,4,\dots} C_{l,n} k^n. \quad (37)$$

The coefficients of the polynomial, $C_{l,n}$, are obtained by collecting powers of k from the sum over the H -polynomial contributions to the second term in Eq. (34). How important are these unreliable contributions? In order to test this, in Figure 10 we calculate $C_{l,n}$ from the $P_l(q)$ multipoles measured from the Nseries simulation boxes (blue and orange for terms up to $l' = 2$ and 18 respectively) and compare to (black dashed)

$$\Delta P_l^{\text{Nseries}}(k) - \Delta P_l^{\text{uncorr}}(k) - \Delta P_l^{\text{corr}}(k) \Big|_{q=0}^{q=k_{\text{trust}}} \quad (38)$$

where $\Delta P_l^{\text{Nseries}}$ is the power spectrum residual $P_l^{\text{NN}} - P_l^{\text{true}}$ for the Nseries mocks (Figure 9). We once again include the standard deviation of the power spectrum residual in shaded gray. The agreement between Eq. (37) and Eq. (38) is more or less equivalent to the agreement seen in Figure 9, which includes uncorrelated and reliable correlated contributions as well; this should of course not come as a surprise.

More importantly, when we examine the contribution to $\Delta P_l^{\text{corr}} \Big|_{k_{\text{trust}}}^{\infty}$ from each individual l' order term of the Eq. (37) polynomial, we find that the main contributors at $k < k_{\text{trust}} \sim 0.3 h/\text{Mpc}$ are the $l' \leq 2$ order terms. In fact, the higher order ($l' > 2$) terms of the polynomial contribute at higher k . For instance, the $l' = 4, 6$, and 8 terms only begin to significantly contribute at scales of $k > 0.3, 0.45$, and $0.6 h/\text{Mpc}$ respectively, which is not surprising since higher k powers come together with increasing inverse powers of q and thus suppress the value of the coefficients that result from integrating over small-scale modes. Hence, when we plot Eq. (37) for just $l' \leq 2$

(blue) in Figure 10, we find that it is in good agreement with both Eq. (37) for $l' \leq 18$ and Eq. (38). We also note that for $l = 2$, $C_{2,l'=0} = 0$ so the main contribution to $\Delta P_2^{\text{corr}}(k < k_{\text{trust}})|_{k_{\text{trust}}}^{\infty}$ comes solely from the $l' = 2$ term of the polynomial.

To use the effective window method for cosmological inference, we can utilize the fact that Eq. (37) with only $l' \leq 2$ terms provides an accurate estimate of the unreliable correlated change in power (Figure 10). In cosmological analyses, the coefficients $C_{l,0}$ and $C_{l,2}$ can be nuisance parameters with priors obtained from mock catalogs. More specifically, for the quadrupole, since $C_{2,0} = 0$ only one nuisance parameter is necessary. Meanwhile for the monopole, a constant shot noise term is typically already included as a nuisance parameter in the analysis (Beutler et al. 2014, 2016; Grieb et al. 2016; Gil-Marín et al. 2016b) so there is also only one extra nuisance parameter for $l = 0$. Therefore, by adding $C_{l,2}$ as nuisance parameters to cosmological inference analyses of the power spectrum multipoles, we can use the effective window method to robustly marginalize over the effects of fiber collision for the entire k range of power spectrum models based on perturbation theory.

4. SUMMARY AND CONCLUSIONS

Using simulated mock catalogs designed specifically for interpreting BOSS clustering measurements with realistically imposed fiber collisions, we demonstrate that the Nearest Neighbor method (NN), most common used for dealing with fiber collisions, is insufficient in accounting for the effect of fiber collisions on the galaxy power spectrum monopole and quadrupole. Although fiber collisions have little significant effect on the power spectrum at large scales, their effect quickly overtakes sample variance on scales smaller than $k \approx 0.1$ h/Mpc . At $k \sim 0.3$ h/Mpc fiber collisions have over a 7.3% and 73% impact on the power spectrum monopole and quadrupole, respectively. The effect is equivalent to 7.3 and 2.5 times the sample variance of CMASS for $\delta k \approx 0.01$ h/Mpc , leading to a binning-independent scale of validity of the NN method of $k_{\chi,2} = 0.068$ h/Mpc for the monopole and $k_{\chi,2} = 0.17$ h/Mpc for the quadrupole (see bottom panel of Figure 7). Consequently at these scales, measurements of the power spectrum becomes dominated by the systematic effects of fiber collisions.

Some recent methods (Beutler et al. 2014; Gil-Marín et al. 2014; Beutler et al. 2016; Grieb et al. 2016; Gil-Marín et al. 2016b) have supplemented the NN method with adjustments to the constant shot noise term in the power spectrum estimator. While these methods improve the overall residual for the monopole, e.g. $k_{\chi,2} = 0.17$ h/Mpc for the method by Gil-Marín et al. (2014), they fail to account for the k -dependence of the systematic effect on smaller scales. Furthermore, since the quadrupole does not have a shot noise term, these methods provide no improvements for $l \geq 2$.

In this paper, we first model the distribution of the line-of-sight displacement between fiber collided pairs using mock catalogs. From the model, we statistically reconstruct the clustering of fiber collided galaxies that reside in the same halo. This, combined with the actual shot noise subtraction of the power spectrum estimator that accounts for chance alignments, leads to our LOS Reconstruction method that recovers very well the true

power spectrum monopole from fiber collided data. As an added advantage, the method only relies on parameters (σ_{LOS} and f_{peak}) measured from the actual observations. This makes the performance of the method independent from the accuracy of the mock catalogs, which are known to be unreliable at small scales.

Using the LOS Reconstruction method, we can recover the true power spectrum monopole to scales well beyond previous methods. The LOS Reconstruction monopole power spectrum residuals remain within sample variance until $k \sim 0.53$ h/Mpc and $k_{\chi,2}$ extends to 0.29 h/Mpc . However, for the power spectrum quadrupole at $k = 0.2$ h/Mpc , the LOS Reconstruction method only reduces the discrepancy between the fiber collided $P_2(k)$ and the true $P_2(k)$ to roughly the sample variance. Therefore, the true monopole power spectrum estimate from the LOS reconstruction method can be compared to the systematics free predicted power spectrum monopole to infer the cosmological parameters of interest without biases from fiber collisions, but for the quadrupole power spectrum the method is not a substantial improvement over previous methods. We trace this problem to the fact that the quadrupole is more sensitive to the object by object finger of god effect, while the LOS reconstruction works only statistically starting from the distribution of close pairs.

To improve on the LOS reconstruction results we develop the effective window method which, rather than attempting to correct the data before making measurements, computes theoretical predictions of the fiber-collided power spectrum multipoles. In this approach, we approximate the effect that fiber collisions have on the two-dimensional configuration space two-point correlation function of the NN method as a scaled top-hat function. Then the effect of fiber collisions can be written as the sum of two contributions: 1) that of uncorrelated chance collisions, with an amplitude proportional to the effective survey area affected by fiber collisions times the wavelength of perturbations, and 2) that of correlated collisions, which is also proportional to the effective survey area affected by fiber collisions and to the integral of the power spectrum over 2D modes perpendicular to the line of sight smoothed at the fiber collision scale.

Using high resolution mock catalogs, we demonstrate that our analytic prescription accurately models the power spectrum residuals from the NN method to within sample variance of BOSS volumes at $k < 0.83$ h/Mpc for both the monopole and quadrupole when the true power spectrum is known down to small scales from simulations, allowing to compute the fiber-collided predictions. Since typically we do not have fast reliable ways of computing the small scale power spectrum, we develop a practical approach when the power spectrum predictions are reliable up to some scale k_{trust} . We split the contributions of the correlated fiber collisions effect into a piece that can be calculated reliably as it depends on large-scale modes, and an unreliable piece that depends on modes that are not under control. We show that the latter piece can be written as polynomials in k , and demonstrate that for scales up to $k \sim 0.3$ h/Mpc , the unreliable contribution can be accurately estimated by a quadratic polynomial in k . In principle, this method can be applied to larger k_{trust} than used here as a reasonable example ($k_{\text{trust}} = 0.3$ h/Mpc).

Therefore, using the effective window method we can model the fiber collided power spectrum as the systematics-free power spectrum plus three contributions due to fiber collisions: an uncorrelated piece (independent of the model power spectrum), a calculable piece (which involves integrating the model power spectrum over 2D long-wavelength modes perpendicular to the line of sight), and an unreliable contribution that is a quadratic polynomial, $C_{l,0} + C_{l,2} k^2$. While the precise values of $C_{l,n}$ cannot be robustly predicted in practice because of its dependence on small scale power, the coefficients can be treated as nuisance parameters in the analysis. Typically a constant shot noise term is already included as a nuisance parameter, while the constant contribution vanishes for higher multipoles, therefore only one extra parameter per multipole is required (the k^2 corrections). For cosmological parameter inference, the fiber collided model power spectrum can be compared directly to the observed fiber collided power spectrum. Then by marginalizing over these free coefficients, we marginalize over the effect of small-scale power induced fiber collisions on the power spectrum, which allows us to robustly infer the cosmological parameters of interest.

The fiber collision correction methods we present will enable us to robustly account for the effects of fiber collisions in galaxy clustering analyses to the smallest scales allowed by theoretical predictions. They can also be extended to future surveys such as eBOSS or any other large fiber-fed surveys that suffer from systematic effects of fiber collisions. Our fiber collision correction method can also be extended to higher order clustering statistics such as bispectrum (Hahn et al., in prep.). We will use the methods presented in this paper to analyze the galaxy power spectrum and bispectrum multipoles in future work.

ACKNOWLEDGEMENTS

CHH and MRB were supported by NSF-AST-1109432 and NSF-AST-1211644. SRT is grateful for support from the Campus de Excelencia Internacional UAM/CSIC. We thank A. I. Malz, Mohammadjavad Vakili, Johan Comparat and particularly David W. Hogg for helpful discussions. CHH also thanks the Instituto de Física Teórica (UAM/CSIC) and particularly Francisco Prada for their hospitality during his summer visit, where part of this work was completed.

REFERENCES

- Alonso, D. 2012, ArXiv e-prints, arXiv:1210.1833 [astro-ph.IM]
 Anderson, L., Aubourg, E., Bailey, S., et al. 2012, MNRAS, 427, 3435
 Behroozi, P. S., Wechsler, R. H., & Wu, H.-Y. 2013, ApJ, 762, 109
 Berlind, A. A., Frieman, J., Weinberg, D. H., et al. 2006, ApJS, 167, 1
 Beutler, F., Saito, S., Seo, H.-J., et al. 2014, MNRAS, 443, 1065
 Beutler, F., Seo, H.-J., Saito, S., et al. 2016, ArXiv e-prints, arXiv:1607.03150
 Bianchi, D., Percival, W., & Bel, J. 2016, ArXiv e-prints, arXiv:1602.02780
 Carretero, J., Castander, F. J., Gaztañaga, E., Crocce, M., & Fosalba, P. 2015, MNRAS, 447, 646
 Chuang, C.-H., Zhao, C., Prada, F., et al. 2015, MNRAS, 452, 686
 Cole, S., Hatton, S., Weinberg, D. H., & Frenk, C. S. 1998, MNRAS, 300, 945
 Colless, M. 1999, Royal Society of London Philosophical Transactions Series A, 357, 105
 Cuesta, A. J., Vargas-Magaña, M., Beutler, F., et al. 2016, MNRAS, 457, 1770
 Dawson, K. S., Schlegel, D. J., Ahn, C. P., et al. 2013, AJ, 145, 10
 Dawson, K. S., Kneib, J.-P., Percival, W. J., et al. 2015, ArXiv e-prints, arXiv:1508.04473
 Feldman, H. A., Kaiser, N., & Peacock, J. A. 1994, ApJ, 426, 23
 Gil-Marín, H., Noreña, J., Verde, L., et al. 2014, ArXiv e-prints, arXiv:1407.5668
 Gil-Marín, H., Percival, W. J., Verde, L., et al. 2016a, ArXiv e-prints, arXiv:1606.00439
 Gil-Marín, H., Verde, L., Noreña, J., et al. 2015, MNRAS, 452, 1914
 Gil-Marín, H., Percival, W. J., Brownstein, J. R., et al. 2016b, MNRAS, 460, 4188
 Grieb, J. N., Sánchez, A. G., Salazar-Albornoz, S., et al. 2016, ArXiv e-prints, arXiv:1607.03143
 Guo, H., Zehavi, I., & Zheng, Z. 2012, ApJ, 756, 127
 Hamilton, A. J. S. 1997, MNRAS, 289, 285
 Hogg, D. W. 1999, ArXiv Astrophysics e-prints, astro-ph/9905116
 Howlett, C., Manera, M., & Percival, W. J. 2015, Astronomy and Computing, 12, 109
 Izard, A., Crocce, M., & Fosalba, P. 2016, MNRAS, 459, 2327
 Kitaura, F.-S., Rodríguez-Torres, S., Chuang, C.-H., et al. 2016, MNRAS, 456, 4156
 Klypin, A., Yepes, G., Gottlober, S., Prada, F., & Hess, S. 2014, ArXiv e-prints, arXiv:1411.4001
 Landy, S. D., & Szalay, A. S. 1993, ApJ, 412, 64
 Makarem, L., Kneib, J.-P., Gillet, D., et al. 2014, A&A, 566, A84
 Manera, M., Scoccimarro, R., Percival, W. J., et al. 2013, MNRAS, 428, 1036
 Manera, M., Samushia, L., Tojeiro, R., et al. 2015, MNRAS, 447, 437
 Maraston, C., Pforr, J., Henriques, B. M., et al. 2013, MNRAS, 435, 2764
 Markwardt, C. B. 2009, in Astronomical Society of the Pacific Conference Series, Vol. 411, Astronomical Data Analysis Software and Systems XVIII, ed. D. A. Bohlender, D. Durand, & P. Dowler, 251
 Monaco, P., Sefusatti, E., Borgani, S., et al. 2013, MNRAS, 433, 2389
 Morales, I., Montero-Dorta, A. D., Azzaro, M., et al. 2012, MNRAS, 419, 1187
 Munari, E., Monaco, P., Sefusatti, E., et al. 2016, ArXiv e-prints, arXiv:1605.04788
 Okumura, T., Hand, N., Seljak, U., Vlah, Z., & Desjacques, V. 2015, Phys. Rev. D, 92, 103516
 Okumura, T., Seljak, U., & Desjacques, V. 2012, JCAP, 11, 014
 Peebles, P. J. E. 1980, The large-scale structure of the universe
 Reid, B. A., Samushia, L., White, M., et al. 2012, MNRAS, 426, 2719
 Rodríguez-Torres, S. A., Prada, F., Chuang, C.-H., et al. 2015, ArXiv e-prints, arXiv:1509.06404
 Ross, A. J., Percival, W. J., Sánchez, A. G., et al. 2012, MNRAS, 424, 564
 Sanchez, A. G., Scoccimarro, R., Crocce, M., et al. 2016, ArXiv e-prints, arXiv:1607.03147
 Sato, M., & Matsubara, T. 2011, Phys. Rev. D, 84, 043501
 Schlegel, D., Abdalla, F., Abraham, T., et al. 2011, ArXiv e-prints, arXiv:1106.1706 [astro-ph.IM]
 Scoccimarro, R. 2015, Phys. Rev. D, 92, 083532
 Scoccimarro, R., & Sheth, R. K. 2002, MNRAS, 329, 629
 Sefusatti, E., Crocce, M., Scoccimarro, R., & Couchman, H. M. P. 2016, MNRAS, arXiv:1512.07295
 Springel, V. 2005, MNRAS, 364, 1105
 Sunayama, T., Padmanabhan, N., Heitmann, K., Habib, S., & Rangel, E. 2016, JCAP, 5, 051
 Takada, M., Ellis, R. S., Chiba, M., et al. 2014, PASJ, 66, R1
 Taruya, A., Bernardeau, F., Nishimichi, T., & Codis, S. 2012, Phys. Rev. D, 86, 103528
 Taruya, A., Koyama, K., Hiramatsu, T., & Oka, A. 2014, Phys. Rev. D, 89, 043509
 Taruya, A., Nishimichi, T., & Bernardeau, F. 2013, Phys. Rev. D, 87, 083509
 Taruya, A., Nishimichi, T., & Saito, S. 2010, Phys. Rev. D, 82, 063522
 Tassev, S., Eisenstein, D. J., Wandelt, B. D., & Zaldarriaga, M. 2015, ArXiv e-prints, arXiv:1502.07751
 Tinker, J. L., Sheldon, E. S., Wechsler, R. H., et al. 2012, ApJ, 745, 16
 White, M., Tinker, J. L., & McBride, C. K. 2014, MNRAS, 437, 2594
 Yan, R., White, M., & Coil, A. L. 2004, ApJ, 607, 739
 Yoon, J. H., Schawinski, K., Sheen, Y.-K., Ree, C. H., & Yi, S. K. 2008, ApJS, 176, 414
 Zehavi, I., Blanton, M. R., Frieman, J. A., et al. 2002, ApJ, 571, 172
 Zehavi, I., Zheng, Z., Weinberg, D. H., et al. 2005, ApJ, 630, 1

APPENDIX

For reference, here we list the first few polynomials $H_{l>l<}(x)$ from Eq. (33)

$$H_{20}(x) = x^2 - 1, \quad (1)$$

$$H_{40}(x) = \frac{7}{4}x^4 - \frac{5}{2}x^2 + \frac{3}{4}, \quad (2)$$

$$H_{42}(x) = x^4 - x^2, \quad (3)$$

$$H_{60}(x) = \frac{33}{8}x^6 - \frac{63}{8}x^4 + \frac{35}{8}x^2 - \frac{5}{8}, \quad (4)$$

$$H_{62}(x) = \frac{11}{4}x^6 - \frac{9}{2}x^4 + \frac{7}{4}x^2, \quad (5)$$

$$H_{64}(x) = x^6 - x^4 \quad (6)$$